Mitochondrial perturbations enhance cell-mediated innate immunity in *Drosophila*

Laura Vesala[1], Yuliya Basikhina[1], Tea Tuomela[1], Pedro F. Vale[2], Tiina S. Salminen[1]

[1]Faculty of Medicine and Health Technology, Tampere University, Tampere, Finland

[2]Institute of Evolutionary Biology, School of Biological Sciences, University of Edinburgh, UK

Corresponding author:

Tiina S. Salminen

tiina.s.salminen@tuni.fi

Abstract

Mitochondria participate in various cellular processes including energy metabolism, apoptosis, stress responses, inflammation and immunity. While mitochondrial dysfunction contributes to many diseases, mitochondrial perturbations can also be beneficial, a phenomenon coined mitohormesis. We investigated how mitochondrial variation contributes to the heterogeneity of infection outcomes and whether moderate mitochondrial dysfunction could benefit immune- challenged individuals. We took three approaches to model variation in mitochondrial oxidative phosphorylation (OXPHOS) in *Drosophila melanogaster*: i) inherited natural mitochondrial DNA (mtDNA) variation present in all tissues; ii) sporadic, tissue-specific silencing of OXPHOS-related genes and iii) systemic pharmacological inhibition of OXPHOS, and studied their effects on the cell-mediated innate immune response. When perturbing mitochondrial function, we detected signs of activated cellular innate immunity without infection and upon infection the perturbation caused enhanced immune response. Our data indicate that mitochondrial dysfunction can be beneficial in immune-challenged individuals when it is mild enough and does not cause complications to the host, and ultimately causes variation in infection outcomes between individuals.

Author summary

Mitochondria are eukaryotic cell organelles involved in various cellular processes including metabolism and cell signaling. The role of mitochondria and the variation of mitochondrial function in immune responses have been increasingly studied across various models. Mitochondrial dysfunction, originating from either the nuclear or the mitochondrial genome, is generally considered harmful for the organism. What is not yet well understood is how immune responses are affected by mitochondrial dysfunction, for example in the context of mitochondrial disease. Here, we show that in the fruit fly *Drosophila melanogaster* mild systemic or immune cell -specific mitochondrial perturbations enhance the innate immune response of the host to parasitoids. Furthermore, we show that due to the mitochondrial perturbations the cell-mediated immune system of the host is activated in the absence of infection and makes the immune responses more efficient upon infection. Importantly, our results demonstrate that mitochondrial genome variation is one of the underlying factors contributing to the variation in infection outcomes among individuals. Our results therefore contribute to the understanding of innate immunity, by providing information about the genetic causes underlying the variation seen in the response to infections.

Short title: Mitochondrial perturbation enhances innate immunity

Keywords

Antimycin A; antioxidant; apoptosis; ATP synthase; cybrid; glycolysis; hemocyte; *HIF-1α*; infection; lamellocyte; *Leptopilina boulardi*; *Ldh*; mitochondrial membrane pontential; mitovariant; mtKSA2; *ND-75*; *ox;* oxidative phosphorylation; reactive oxygen species; *sima*

Introduction

Eliciting an effective immune response requires coordinated changes in metabolism, including the mobilization and allocation of energy reserves. Mitochondria have a central role in the metabolic control of immune responses as it produces energy via oxidative phosphorylation (OXPHOS), a primary function that is conserved in eukaryotes. OXPHOS is composed of five protein complexes (cI-cV), located at the inner membrane of the double-membraned mitochondria, and each of these complexes (except cII) contains subunits encoded both by the mitochondrial genome (mtDNA) and the nuclear genome. During the past decade, the role of mitochondria in innate and adaptive immune responses has been increasingly studied and mitochondria have been shown to participate in immune responses in several ways e.g. by controlling apoptosis, regulating various signaling molecules and pathways and by producing reactive oxygen species (ROS) [1–6]. Depending on the phase of the immune response and the tissue/cell type in question, the metabolic reprogramming can lead to favouring cytosolic aerobic glycolysis instead of mitochondrial OXPHOS [7–11]. A well-known example of this kind of metabolic switch occurs in inflammatory macrophages, which favor aerobic glycolysis over OXPHOS [12,13], a phenomenon referred as the Warburg effect [14].

As mitochondria contain their own maternally inherited circular genome, their functions rely on the coordinated signaling between the nuclear and mitochondrial genomes, and mutations in one or both genomes can lead to variation in mitochondrial functions. This variation, in turn, contributes to the variation in a plethora of phenotypes shown in different organisms (for example [15–18]). In some cases, mutations can hamper the mitochondrial function and result in mitochondrial diseases [19], the severity of which vary depending on the mutation, the affected tissues [20] and on compensatory mechanisms arising from (and depending on) the particular nuclear and mitochondrial genomes and their interactions. Since mitochondrial dysfunction is involved in several pathologies, including

101 neurodegenerative diseases, metabolic disorders such as diabetes, myopathies and multiorgan failure,
102 mitochondrial and nuclear mutations leading to disruption in mitochondrial function could be
103 expected to be harmful in the context of immunity. Although immune responses have not yet been
104 much studied in connection with mitochondrial diseases, the evidence does point towards a link
105 between mitochondrial disease and immunodeficiency (reviewed in [21]). This has also been shown
106 in a fruit fly *Drosophila melanogaster* model with compromised OXPHOS due to an incompatible
107 interaction between the mt-$tRNA_{Tyr}$ and mt-tyrosyl-tRNA synthetase variants encoded by the
108 mitochondrial and the nuclear genomes, respectively. This incompatibility, and compromised
109 OXPHOS, was shown to cause a reduction in innate immune response when *Drosophila* females
110 were exposed to a bacterial pathogen [22].

111

112 Salminen et al. [23] showed with *D. melanogaster* that a naturally occurring mtDNA variant called
113 mtKSA2 with a mutation in the OXPHOS cIII gene *cytochrome b* (*cyt-b*) caused the formation of
114 melanotic nodules when introgressed into different nuclear backgrounds. Melanotic nodules are
115 melanised masses of *Drosophila* blood cells (hemocytes), and they are considered to signify an
116 (aberrantly) activated immune system [24]. These findings made us ask whether moderate
117 mitochondrial dysfunction at the systemic and/or tissue level could enhance immune responses,
118 possibly acting through activation of the immune system prior infection or through mitohormesis
119 where mitochondrial perturbance causes favourable changes in the expression of nuclear genes [25].
120 To answear this question, we utilized the *Drosophila* model which lacks the adaptive immunity, but
121 has long been used as a model for studying the innate immunity, due to the conservation of signaling
122 cascades and effector molecules between the fly and humans (reviewed in [26]). The fly's innate
123 immune effector cells, the hemocytes, are produced in two waves during development: the embryonic
124 and larval hematopoiesis [27]. At the larval stages, the hemocyte system consists of phagocytic cells
125 called plasmatocytes, which bear functional similarities to mammalian macrophages [28] and an

immune-inducible hemocyte type called the lamellocyte [29,30]. Lamellocytes are large discoidal cells and they encapsulate pathogens that are too large for phagocytosis. Lamellocytes are also involved in the formation of the aforementioned melanotic nodules via aggregating and producing melanin [24]. A third hemocyte type, the crystal cell, function mainly in wound healing and are present in relatively low numbers in larvae and adults [31,32]. All larval hemocyte types are produced from progenitor cells in an organ called the lymph gland [33], and lamellocytes also transdifferentiate from mature plasmatocytes in the circulation carried over from the embryo to the larval stage [34–36].

We harnessed three approaches to study the effect of variation in mitochondrial function on cell-mediated innate immune response. First, to investigate the effect of natural mtDNA mutations that are inherited maternally and are present in each tissue of the host, we used the *Drosophila* cybrid (cytoplasmic hybrid) model where mtDNA variants have been introgressed into controlled nuclear background. Second, to study the effect of spontaneous tissue-specific mutations, we silenced selected nuclear-encoded genes of each of the five OXPHOS complexes tissue-specifically. Finally, we used a pharmacological approach to inhibit the function of OXPHOS. We show that moderate OXPHOS perturbations either at the organismal level or in immune cells have a beneficial effect on the innate immunity of the fly.

Results

The natural mtDNA variant mtKSA2 has an enhanced cell-mediated innate immune response against the parasitoid wasp *Leptopilina boulardi*

The effects of naturally occurring variation in the mitochondrial genome (mtDNA) on immunity are unclear, partially due to the challenges of separating the mtDNA effects from those arising from the

151 nuclear DNA [4]. We utilized *Drosophila* cybrid (cytoplasmic hybrid) strains where unique mtDNA
152 variants have been introgressed onto an isogenic nuclear background to separate the effect of variation
153 in the nuclear genome from that arising from the mtDNA [37]. A naturally occurring mtDNA variant
154 (called mtKSA2) was previously shown to cause the formation of melanotic nodules in *Drosophila*
155 cybrid larvae in different nuclear backgrounds [23]. This motivated us to examine if mtDNA variation
156 and specifically the mtKSA2 variant has an impact on the cell-mediated innate immune response and
157 the outcome of an infection. Using a parasitoid wasp *L. boulardi* infection, we induced the cell-
158 mediated immune response in the larvae of four strains containing unique mtDNA variants, mtORT,
159 mtWT5A, mtBS1 and mtKSA2 (S1 Table) in an ORT nuclear background.
160
161 We measured the efficiency of the immune response against parasitoid wasps as a proportion of
162 melanised wasp larvae found in cybrid larvae reared at 25 °C and 29 °C. In general, fully (+)
163 melanised wasp larvae were scarce in all four strains when reared at 25 °C, ranging from 0 % in the
164 mitovariants mtORT and mtWT5A to 5 % in mtBS1 and 9 % in mtKSA2 (Fig 1A, light purple).
165 Rearing the larvae at 29 °C improved the efficiency of the encapsulation response especially in
166 mtKSA2 larvae, as they were now able to melanise (both partially and fully) more wasp larvae than
167 the other cybrid strains at this temperature (Fig 1A, dark purple). These results show that there is
168 mitovariant-specific variation in the immune response against parasitoid wasps, and that the mtKSA2
169 larvae are able to elicit a more efficient immune response compared to the other tested mitovariants.
170
171 **mtKSA2 larvae show signs of enhanced aerobic glycolysis**
172 Given the elevated parasitoid melanisation in the mtKSA2 larvae, we focused on this strain to explore
173 the underpinnings of mtDNA-mediated enhancement of cellular immunity. mtKSA2 harbours the
174 mutation D21N in the mtDNA encoded *cytochrome b* (*cyt-b*) gene of the OXPHOS cIII, which has
175 been predicted to destabilize the interactions between the subunits of cIII, based on crystal structure

176 models [23]. mtKSA2 also has another mutation (A75T) in the cIV gene *Cytochrome c oxidase*
177 *subunit III* (*COIII)*, but the possible effects of this mutation have not been characterized [23]. We
178 reasoned that the *cyt-b* mutation may lead to impaired OXPHOS function, which, in turn, may lead
179 to a switch from mitochondrial respiration to favour cytosolic aerobic glycolysis as the source of
180 energy. If this is the case, the larvae may need to mobilize their storage sugars to meet the increased
181 glucose demand. Therefore, we measured the levels of the storage sugar glycogen in the cybrid larvae.
182 As female and male *Drosophila* may have differences in their metabolism [38], sexes were analysed
183 separately. mtKSA2 larvae, especially females, showed a trend for decreased levels of glycogen
184 storages when compared the other cybrid strains, but the differences were not statistically significant
185 (Fig 1B-B'). Since differences in feeding among the larvae may affect the ability to built up glycogen
186 storages, we next checked the larval gut contents as a proxy of food intake. The trend for reduced
187 glycogen was not explained by reduced feeding, since mtKSA2 males had more gut content than the
188 other cybrids, and also mtKSA2 females had increased gut content compared to the mtORT females,
189 but not in comparison to mtBS1 or mtWT5A females (S1A-B Fig). Of note, the size of the larvae,
190 based on the protein content in the samples, did not statistically significantly differ between the cybrid
191 larvae, indicating that there are no major defects in their food consumption/metabolism that would
192 affect the growth of the animals (S1C Fig). But it is noteworthy that mtKSA2 and mtORT male larvae
193 were smaller than the respective females, which was not the case for mtBS1 and mtWT5A larvae
194 (S1C Fig).
195
196 To further disentangle the glycolytic state of the larvae, we measured the expression levels of the
197 transcription factor *similar* (*sima*) and its target *Lactate dehydrogenase* (*Ldh*) in the cybrid larvae.
198 The expression of both genes has been shown to be increased in *Drosophila* when cells shift to utilize
199 aerobic glycolysis [39]. *Sima* expression was elevated in mtKSA2 male larvae when compared to the
200 other cybrids, and also in females in comparison to mtORT and mtWT5A (Fig 1C-C'). However,

201 there were no detectable changes in the expression of Sima's target gene *Ldh* among the cybrids (Fig
202 1D-D').
203
204 Taken together, mtKSA2 flies showed a trend towards smaller glycogen reservoirs and they had more
205 food content in their guts at the 3rd instar stage than other cybrids, which may indicate that the
206 mtKSA2 flies utilize their glycogen storages more and possibly feed more as an attempt to replenish
207 the reduced glycogen storages. This, together with the increased expression levels of *sima* in the
208 mtKSA2 larvae suggests an increased utilization of aerobic glycolysis in these animals.
209
210 **mtKSA2 larvae have a higher hemocyte count and elevated hemocyte ROS**
211 As the encapsulation response against the parasitoid wasps requires hemocyte proliferation and
212 differentiation of a specialized immune-activated hemocyte type (the lamellocyte), we tested the
213 amounts and types of hemocytes in the cybrid larvae. We applied flow cytometry to assess the total
214 number of circulating hemocytes in uninfected and *L. boulardi* -infected cybrid larvae (S2A-C' Fig).
215 In general, we did not observe sex-differences in hemocyte numbers, apart from wasp-infected
216 mtKSA2 males, which had slightly more hemocytes than females at 29 °C (S2D-E' Fig). Therefore,
217 the hemocyte data was pooled for the subsequent analyses. We found that uninfected mtKSA2 larvae
218 had higher hemocyte counts than the other strains at both temperatures (Fig 2A), and at 29 °C this
219 was the case also after wasp infection (Fig 2B). Taking advantage of the morphological difference
220 between plasmatocytes (round cells) and lamellocytes (flat and discoidal cells), we sub-gated the total
221 hemocytes in two groups in an FSC-Area (FSC-A) vs. FSC-Height (FSC-H) plot. Plasmatocytes (or
222 any round cell) form a population roughly at a 45° angle in the FSC-A vs FSC-H plot due to having
223 an equal ratio between height and area. We gated the cells that deviated from this ratio and called the
224 gate the "activated hemocyte gate" (S2C-C' Fig). More mtKSA2 hemocytes were in this gate both in
225 uninfected and wasp-infected larvae reared at 29 °C than in the other cybrid strains (Fig 2A' & B').

226 To test if the differences in the hemocyte numbers might be due to the differences in the hemocyte
227 viability, we analysed the proportion of living hemocytes (PI-negative) out of a total amount of
228 hemocytes detected in the main hemocyte gate. There were no sex-specific differences in hemocyte
229 viability and also the strain-specific differences were small (S2F-G' Fig). mtKSA2 larvae had a
230 slightly higher proportion of live hemocytes than mtORT larvae in all conditions except for in
231 uninfected larvae reared at 29 °C, where there was no difference (S2F-G' Fig).
232
233 We further tested for the presence of mature lamellocytes by measuring the expression of
234 *prophenoloxidase 3* (*PPO3*) in the hemocytes of uninfected mtORT and mtKSA2 larvae maintained
235 at 29 °C. *PPO3* is expressed in lamellocytes and encodes for an enzyme required in the melanisation
236 response [40]. We did not detect differences in the expression levels of *PPO3* between the studied
237 strains (Fig 2C). Therefore, it remains somewhat uncertain if the mtKSA2 mitovariant, besides
238 increasing the total hemocyte numbers, also induces lamellocyte formation, or perhaps affects some
239 other aspect of hemocyte activation that is beneficial for the cellular immune response.
240
241 Finally, we measured the levels of reactive oxygen species (ROS) in hemocytes from the four cybrid
242 strains, as ROS is tightly linked to immune activation, and the *cyt-b* mutation found in mtKSA2 may
243 affect ROS production via its effects on the function of OXPHOS cIII. The basal level ROS was
244 measured with the CellROX™ green probe (S3A-C Fig) from hemocytes of pooled uninfected larvae
245 reared at 29 °C. Results showed that the mtKSA2 larvae had the highest proportion of CellROX-
246 positive hemocytes (Fig 2D).
247
248 Taken together, mitovariant mtKSA2 has multiple effects on the larval physiology. The effects on
249 aerobic glycolysis, immune cell composition and ROS production in the immune cells result in an

250 improved cell-mediated immune response in mtKSA2 larvae upon wasp infection, possibly caused
251 by a subtle cell-mediated immune activation prior to infection.
252
253 **Knocking down OXPHOS complex genes ubiquitously or in the fat body, but not in the**
254 **hemocytes, has drastic effects on the viability of the flies**
255 As mtKSA2 contains two unique non-synonymous point mutations in OXPHOS complexes III and
256 IV (S1 Table) [23,37], we examined if the immune protective phenotype is restricted to cIII or cIV
257 variation or if it is a more general phenomenon related to OXPHOS function. To test this, we
258 individually knocked down nuclear genes encoding for OXPHOS complex I-V (cI-cV) proteins
259 tissue-specifically, as we hypothesized that depending on the tissue, the effect of the knockdowns on
260 the host's viability would vary in severity.
261
262 We chose one or two genes of each of the five OXPHOS complexes for knockdown experiments
263 from the two VDRC RNAi libraries (Fig 3A, S2 Table). We first tested the viability of the animals
264 when these genes were individually knocked down ubiquitously (*da-GAL4*), from the fat body (*Fb-*
265 *GAL4*) or hemocytes (*Hml$^{\Delta}$-GAL4;He-GAL4*). When the genes were knocked down in the whole
266 animal, all of them manifested severe developmental delay at the larval stages and were eventually
267 lethal (S3 Table). In the case of the fat body-specific gene silencing, the effects varied from mild
268 developmental delay to lethality. The development of *ND-75* (cI) and *SdhD* (cII) fat body knockdown
269 animals was delayed but they were able to eclose, and in *ox* (cIII), *UQCR-C1* (cIII), *COX5B* (cIV)
270 and *ATPsynC6* (cV) the knockdown caused partial or complete lethality at the pupal stage (S3 Table).
271
272 However, knocking down the OXPHOS cI-cV specific genes from the hemocytes did not affect the
273 development rate or viability when compared to controls. Given the central role of hemocytes in the
274 cell-mediated innate immunity, the observation of melanotic nodules in the mtKSA2 variant [23] and

275 our finding that mtKSA2 had more hemocytes and potential hemocyte activation in the absence of
276 infection (Fig 2A-A'), we focused our studies on larval hemocytes and the effect of decreased
277 OXPHOS function in hemocytes on cell-mediated innate immune response.
278
279 **Knockdown of nuclear OXPHOS complex genes in hemocytes induces the formation of**
280 **melanotic nodules and hemocyte activation**
281 We expressed the OXPHOS RNAi constructs (Fig 3A) in hemocytes (*Hml$^{\Delta}$-GAL4;He-GAL4/UAS-*
282 *OXPHOS RNAi*) and checked for the presence of melanotic nodules from 3rd instar larvae reared at
283 29 °C. Examples of the most common type of melanotic nodules scored in the experiments are shown
284 in Fig 3B-B''. We found that silencing the OXPHOS cIII, cIV and cV genes in hemocytes caused the
285 formation of melanotic nodules. The prevalence of the nodules ranged from 8 to 14 % in the GD
286 library RNAi strains and from 2 to 31% in larvae from the KK library strains (Fig 3C). *ND-75* (cI)
287 knockdown caused only a mild melanotic nodule phenotype, resulting a nodule prevalence of 2 % in
288 the GD strain and 1 % in the KK strain. Another exception was the cII gene *SdhD* whose knockdown
289 in hemocytes caused nodules in 1 % in the GD strain and no nodules in the KK strain).
290
291 Having established a link between the formation of melanotic nodules and OXPHOS dysfunction in
292 hemocytes, and considering that the mitovariant mtKSA2 exhibited both nodules [23] and enhanced
293 immune response against parasitic wasps (Fig 1A), we hypothesized that both of these phenomena
294 could be explained by hemocyte differentiation. Therefore, we checked if silencing the OXPHOS
295 genes in hemocytes affected hemocyte numbers and/or types. We utilized the *in vivo* hemocyte
296 reporter system (*eater-GFP* and *msn-mCherry*) to identify five hemocyte populations based on the
297 levels of the GFP and mCherry fluorescence [34]. In uninfected *msn-mCherry,eater-GFP;Hml$^{\Delta}$-*
298 *GAL4;He-GAL4/w^{GD}* larvae (control), as expected mainly hemocytes expressing high levels of *eater-*
299 *GFP* (plasmatocytes) were present (Fig 4A). Knocking down genes of OXPHOS complexes I, III, IV

300 and V resulted in hemocyte activation as uninfected larvae produced infection-specific hemocytes,
301 including lamellocytes, which express high levels of *msn-mCherry* and do not express the
302 plasmatocyte marker *eater-GFP* (Fig 4A-B). In this context complex II behaved as an outlier, as the
303 knockdown of *SdhD* did not induce hemocyte activation (Fig 4A-B). Most of the OXPHOS gene
304 knockdowns also resulted in an increase of total hemocyte numbers, but this effect was more
305 inconsistent than the hemocyte activation phenotype (including lamellocyte formation), which tended
306 to get stronger the further along the OXPHOS complex chain the knockdown was (Fig 4B).
307
308 For the follow-up studies we selected genes encoding for the OXPHOS cI core component *NADH*
309 *dehydrogenase (ubiquinone) 75 kDa subunit* (*ND-75*), cIII component *oxen* (*ox*) and cV stalk subunit
310 *ATP synthase, coupling factor 6* (*ATPsynCF6*). We selected the VDRC GD library RNAi constructs
311 for these genes and first verified that they efficiently silenced the expression of their target gene
312 (*Hml$^{\Delta}$-GAL4;He-GAL4/UAS-OXPHOS RNAi* vs. *Hml$^{\Delta}$-GAL4;He-GAL4/w^{GD}*). *ND-75* and
313 *ATPsynCF6* expression was significantly reduced in the knockdown strains (S4A-A' Fig).
314 Unfortunately, we were not able to measure the RNAi efficiency of *ox*, as the RNAi construct's
315 hairpin sequence covers the majority of the gene, leaving no space to design proper qPCR primers
316 for the remaining gene sequence. We also measured the RNAi efficiency of the cII gene *SdhD* that
317 did not show the phenotypes observed with other OXPHOS component knockdowns (Figs 3C and
318 4A-B). Both GD an KK *SdhD* RNAi strains showed strong reduction in *SdhD* expression (S4A-A'
319 Fig).
320
321 A detailed view of the hemocyte profiles from these selected gene knockdowns is shown in Fig 4C-
322 C''''', and that of the rest of the lines is shown in S5A-D'' Fig. Knocking down *ATPsynCF6* (cV)
323 resulted in an increase in total hemocyte numbers, mainly explained by the increase in plasmatocytes
324 (Fig 4C-C'). All selected OXPHOS gene knockdowns resulted in the increase of activated

325 plasmatocytes (Fig 4C''), which are characterized by high *eater-GFP* and moderate *msn-mCherry*
326 [34]. In addition, *ox* (cIII) and *ATPsynCF6* knockdowns resulted in the formation of prelamellocytes,
327 hemocytes characterized with low *eater-GFP* expression together with moderate expression of *msn-*
328 *mCherry* and mature lamellocytes, while knocking down *ND-75* (cI) did not (Fig 4C''''-C'''''). Of
329 note, knocking down *ND-75* using the KK library construct did result in the formation of
330 prelamellocytes and lamellocytes (Fig 4B, S5 Fig), indicating that cI silencing may also induce
331 lamellocyte formation. Lamelloblasts, which are putative lamellocyte precursors [34], were elevated
332 only upon *ATPsynCF6* knockdown (Fig 4C''').
333
334 In conclusion, disrupting the function of the OXPHOS complex by silencing complex-specific genes
335 in the whole animal or in the fat body is detrimental, but silencing them in hemocytes does not affect
336 egg-to-adult survival. Furthermore, hemocyte-specific OXPHOS RNAi resulted in the formation of
337 melanotic nodules and, for most of the complexes, in hemocyte activation including the generation
338 of lamellocytes in the absence of infection.
339
340 **Silencing OXPHOS cI, cIII and cV -related genes leads to a loss of mitochondrial membrane**
341 **potential and reduced apoptosis in hemocytes**
342 To verify that silencing the selected OXPHOS genes resulted in an alteration in mitochondrial
343 function, we measured the mitochondrial membrane potential (ΔΨm), as a readout of mitochondrial
344 activity in the hemocytes. For this, we used a TMRM dye and flow cytometry. As a control we treated
345 hemocytes from *msn-mCherry,eater-GFP;Hml$^{\Delta}$-GAL4;He-GAL4/w^{GD}* larvae with carbonyl cyanide
346 3-chlorophenylhydrazone (CCCP), an uncoupler of oxidative phosphorylation in mitochondria, and
347 compared the signal to untreated hemocytes (Fig 5A). We compared only the *eater-GFP*-expressing
348 plasmatocytes to avoid possible hemocyte type -specific effects related to the mitochondrial
349 membrane potential. When comparing the plasmatocytes of *ND-75*, *ox* or *ATPsynCF6* silencing (*msn-*

350 *mCherry,eater-GFP;Hml$^{\Delta}$-GAL4;He-GAL4/UAS-OXPHOS RNAi*) to the controls, we found that *ox*
351 and *ATPsynCF6* knockdown showed significantly lower MitoProbe signal intensity, indicating loss
352 of membrane potential (Fig 5A'-A''). In the *ND-75* knockdown plasmatocytes the reduction in the
353 MitoProbe signal was milder (and statistically not significant) than the reduction seen in *ox* and
354 *ATPsynCF6* knockdown hemocytes. Also in the case of cII gene *SdhD* the knockdown did not result
355 in the loss of mitochondrial membrane potential but instead there was a small but non-significant
356 elevation of the membrane potential (Fig 5B-B').
357
358 Since mitochondrial signaling is involved in the regulation of apoptosis and the rate of apoptosis can
359 be affected by the loss of membrane potential, we checked if the silencing of OXPHOS genes leads
360 to changes in the amount of apoptotic hemocytes. As a positive control, we treated the *msn-*
361 *mCherry,eater-GFP;Hml$^{\Delta}$-GAL4;He-GAL4/w^{GD}* hemocytes with CCCP to induce apoptosis, and saw
362 that the signal of the Annexin V pacific blue conjugate, used to detect cells at an early stage of
363 apoptosis, increased in the treated hemocytes as expected (Fig 5C). In contrast, silencing *ox* and
364 *ATPsynCF6* led to a reduction in the amount of hemocytes positive for the Annexin V stain compared
365 to the controls, whereas *ND-75* knockdown did not have an effect on the rate of apoptosis (Fig 5C'-
366 C''). Of note, dead cell staining of hemocytes did not reveal differences in the viability among the
367 OXPHOS gene knockdown and control hemocytes (Fig 5D).
368
369 In conclusion, the silencing of the *ox* (cIII) and *ATPsynCF6* (cV) genes in hemocytes led to the
370 perturbation of mitochondrial function indicated by the loss of membrane potential accompanied with
371 reduced apoptosis, but not in any changes in the viability of the hemocytes.
372

373 **OXPHOS gene knockdown in hemocytes does not lead to conclusive changes in sugar**
374 **metabolism but *ox* and *ATPsynCF6* knockdown induce the expression of *Ldh* as a sign of**
375 **increased aerobic glycolysis in hemocytes**

376 Next, we investigated whether a switch to aerobic glycolysis in hemocytes could be behind the
377 hemocyte activation seen accompanying OXPHOS perturbation. We compared the levels of glycogen
378 and trehalose in *ND-75*, *ox* and *ATPsynCF6* knockdown larvae to those in the controls, sex
379 specifically. We hypothesized that in the knockdown larvae there would be a decrease in glycogen
380 levels, as the storage sugars are mobilized to feed glucose into accelerated glycolysis. This, in turn,
381 might be reflected in the levels of trehalose in the hemolymph, which is the main circulating sugar in
382 *Drosophila* larvae. We found that the glycogen levels in the OXPHOS knockdown larvae did not
383 significantly differ from the controls (Fig 6A-A'). The levels of hemolymph trehalose were increased
384 when *ND-75* was silenced in hemocytes, but only in females, and decreased in male *ox* knockdown
385 larvae (Fig 6B-B').

386

387 Next, we measured the gene expression levels of *sima* and *Ldh* in hemocytes as indicators of aerobic
388 glycolysis. While *sima* expression was unaffected, or even reduced in the case of *ND-75* and
389 *ATPsynCF6* knockdown hemocytes in males (Fig 6C-C'), its transcriptional target gene *Ldh* was
390 upregulated in hemocytes with *ox* and *ATPsynCF6* silencing, and slightly also in *ND-75* knockdown
391 males (Fig 6D-D'). Since knockdown of the cII gene *SdhD* did not lead to the formation of melanotic
392 nodules nor in hemocyte activation, we checked the knockdown effects on the expression of *sima* and
393 *Ldh*. *SdhD* silencing in hemocytes did not affect the expression of *sima* (Fig 6C-C'), similarly to *ND-*
394 *75*, *ox* and *ATPsynCF6* knockdowns, and it also did not alter the *Ldh* expression (Fig 6D-D').

395

396 Taken together, OXPHOS perturbation in hemocytes did not drastically alter the sugar metabolism,
397 as no consistent changes in the glycogen or trehalose levels or *sima* expression were found. However,

398 the *sima* target gene *Ldh* showed elevated expression in *ox* and *ATPsynCF6* knockdown hemocytes.
399 These results suggest that although no major changes in the sugar metabolism were observed, the
400 elevated levels of *Ldh* could indicate an increase in glycolysis in the cIII and cV knockdown
401 hemocytes.
402
403 **Knocking down OXPHOS genes in hemocytes enhances the cell-mediated encapsulation**
404 **response against parasitoid wasps**
405 Since we found that the cell-mediated immune response was enhanced in the mtKSA2 larvae, we
406 tested if the same effect could be achieved with the OXPHOS complex I-V gene knockdowns in
407 hemocytes. To that end, we infected the larvae with OXPHOS gene silencing in their hemocytes
408 (*Hml$^{\Delta}$-GAL4;He-GAL4/UAS-OXPHOS RNAi*) with *L. boulardi* parasitoid wasps and scored the
409 percentage of larvae with a completely successful immune response against the wasps (fully
410 melanised wasp larvae). Indeed, none of the knockdowns lowered the immune response and many of
411 them resulted in enhanced melanisation and encapsulation of the wasp larvae, when compared to the
412 controls (*Hml$^{\Delta}$-GAL4;He-GAL4/w*; Fig 7A). Here, as an additional control, we also crossed the
413 OXPHOS RNAi strains to the *w^{1118}* background (*w^{1118}/OXPHOS RNAi*). Overall, the response against
414 wasps in the OXPHOS knockdown larvae was enhanced or stayed the same also when compared to
415 these RNAi strain -specific controls, with the exception of knockdown of the complex II (Fig 7A).
416 Despite some strain and/or background -specific variation in the encapsulation response, overall
417 tendency was towards enhanced encapsulation response. On the contrary, when we knocked down
418 *ND-75* and *ATPsynCF6* from another tissue important for the *Drosophila* immune response, the fat
419 body, the melanisation response against wasps was drastically reduced (Fig 7B). As the immune-
420 enhancing effect was shown to be hemocyte-specific, we tested if hemocyte-specific OXPHOS
421 silencing has any additional effects on the hemocyte populations at 48 hours after wasp infection
422 compared to wasp-infected controls. Overall, the larvae with OXPHOS silencing in hemocytes had a

423 similar hemocyte profile as the wasp-infected controls, including similar amounts on lamellocytes
424 (S6A-A''''' Fig). The only exception to this was a small reduction in the activated plasmatocyte
425 population in *ox* knockdown larvae after infection (S6A'' Fig).
426
427 These results indicate that OXPHOS perturbations with mild effects on the host viability such as in
428 the case of hemocytes can be beneficial for the host upon a immune challenge, whereas OXPHOS
429 dysfunction causing more severe stress as in the case of fat body, is immune-suppressing.
430
431 **Immune beneficial effect of OXPHOS gene silencing is not due to changes in levels of ROS**
432 The disruption of OXPHOS, especially complexes I and III, leads to increased electron escape,
433 creating increased amounts of ROS (reviewed in [41]). We measured the levels of ROS in the
434 OXPHOS cI, cIII and cV knockdown hemocytes using the CellROX™ green probe. We fed the
435 antioxidant N-acetylcysteine (NAC) to the larvae as a negative control (to reduce ROS) and compared
436 the CellROX green signal in hemocytes from NAC-fed larvae to that of the control hemocytes (Fig
437 7C). The OXPHOS complex I, III and V knockdown hemocytes (*Hml$^{\Delta}$-GAL4,He-GAL4/UAS-*
438 *OXPHOS RNAi*) did not differ in their levels of ROS from the controls (*Hml$^{\Delta}$-GAL4,He-GAL4/w^{GD}*)
439 when measured as the CellROX green signal intensity (Fig 7C'-C'') or as a percentage of hemocytes
440 positive for the CellROX signal (Fig 7C''').
441
442 We studied further the role of ROS in hemocytes, and whether elevating the levels of ROS in
443 hemocytes could phenocopy the effects of the OXPHOS RNAi on the formation of melanotic
444 nodules, hemocyte activation and the immune response against wasps. To this end, we knocked down
445 genes encoding for enzymes with antioxidant function; *Superoxide dismutase 1* and *2* (*Sod1* and
446 *Sod2*) and *Catalase* (*Cat*) from larval hemocytes. *Sod2* converts superoxide to hydrogen peroxide in
447 the mitochondria, whereas *Sod1* functions in the cytosol [42,43]. Catalase is the only enzyme

448 breaking down hydrogen peroxide in *Drosophila*, and it is expressed in the cytosolic compartment of
449 the cell [44]. Knocking down the antioxidant genes in hemocytes did not cause the formation of
450 melanotic nodules (0 % prevalence in *Sod1* and *Sod2* knockdowns, 1 % in *Cat* knockdown, data not
451 plotted), and only knocking down *Sod1* with the GD library construct influenced the melanisation
452 response against wasps by enhancing it slightly (Fig 7D). Furthermore, knocking down the
453 antioxidant genes did not result in hemocyte activation nor lamellocyte formation (Fig 7E-E'''''),
454 indicating that the antioxidant RNAi does not phenocopy the effect of the OXPHOS RNAi on
455 immune cell activation. Interestingly, the amount of hemocytes expressing low levels of *eater-GFP*
456 (lamelloblasts) was elevated in all three antioxidant gene knockdowns (Fig 7E''').
457
458 Based on these results, OXPHOS complex I, III and V gene knockdowns do not alter the levels of
459 ROS in larval hemocytes. Furthermore, knocking down genes encoding for antioxidants did not result
460 in similar effects on the immune response as did the silencing of OXPHOS genes, further indicating
461 that these effects are not mediated by increased mitochondrial ROS production, but rather via some
462 other mechanism launched by reduced OXPHOS activity.
463
464 **Pharmacological inhibition of complex III partially phenocopies the mtKSA2 effect**
465 Partial inhibition of the function of OXPHOS cIII with antimycin A has been shown to cause the
466 formation of melanotic nodules in otherwise healthy cybrid larvae and to be sub-lethal when
467 combined with the mitovariant mtKSA2 that possess a cIII mutation [23]. Here, we tested whether
468 we can phenocopy the effect of the mtKSA2 mutation by pharmacologically inhibiting the cIII
469 function with antimycin A. We aimed to induce mild mitochondrial perturbation to the cybrid nuclear
470 background strain ORT and the RNAi background strain w^{GD} by feeding the larvae different
471 concentrations of antimycin A and checking the larvae for the presence of melanotic nodules as a
472 sign of phenocopy. Using the concentrations 4, 6 and 8 ug/ml gradually increased the percentages of

473 melanotic nodules in the ORT and w^{GD} larvae. However, there was a significant background effect
474 on the sensitivity to the antimycin A treatment as ORT produced more nodules in each of these
475 concentrations when compared to w^{GD} (Fig 8A). As we aimed to cause a mild cIII perturbation, we
476 continued with the w^{GD} line and an antimycin A concentration of 6 ug/ml. Feeding antimycin A led
477 to a reduced melanisation response against wasps (Fig 8B) and did not have an effect on the hemocyte
478 counts in the w^{GD} larvae (Fig 8C-C'). We also fed 6 ug/ml antimycin A to *msn-mCherry,eater-*
479 *GFP;Hml*$^{\Delta}$*-GAL4;He-GAL4/*w^{GD} larvae and analysed the hemocyte populations based on *eater-GFP*
480 and *msn-mCherry* expression. In this context, there was an increase of total hemocytes (mainly due
481 to increased plasmatocyte counts) in antimycin A -fed larvae reared at 29 °C, but no hemocyte
482 activation was detected (Fig 8D-D'''''').
483
484 **Discussion**
485
486 Responses to a pathogen can vary widely among individuals due to multiple factors, such as the age
487 or sex of the individual, earlier pathogen exposure and various genetic factors (reviewed in [45–47]).
488 Here, we studied whether mitochondrial variation, more specifically in oxidative phosphorylation
489 (OXPHOS), causes variation in cell-mediated innate immune responses. Since OXPHOS is a core
490 mitochondrial function, we aimed at eliciting relatively mild OXPHOS perturbations and studying
491 their effects on the immune activation and infection outcome. By combining various methods we
492 modelled the systemic effect of uniparentally inherited mtDNA mutations and pharmacological
493 inhibition of OXPHOS, as well as the effect of sporadic, tissue-specific mitochondrial mutations
494 originating from the nuclear genes via targeted gene silencing. Fig 9 shows the summary of our main
495 findings.
496
497

498 *Melanotic nodules are a general feature of OXPHOS dysfunction*

499 The common feature among the three models of mitochondrial perturbation was the formation of
500 melanotic nodules. Melanotic nodules (also called melanotic pseudotumours) are formed via the
501 activity of the specialized hemocytes, the lamellocytes [24], either as a response to self (an
502 autoimmune response) or because of the aberrant activation of the hemocytes [24,48–50]. mtKSA2
503 mitovariant with a cIII (cyt-b) mutation was originally shown to harbour melanotic nodules when it
504 was present in its original KSA2 nuclear background and when introgressed into a healthy or a
505 mitochondrially sick ORT background [23]. Furhermore, pharmacological inhibition of cIII with
506 antimycin A was shown to cause melanotic masses in each tested Drosophila line and to be semilethal
507 in the presence of mitovariant mtKSA2 [23]. Here, we show that the nodule phenotype is not cIII -
508 specific, as knocking down nuclear encoded OXPHOS cI, cIII, cIV and cV genes in hemocytes also
509 led to the formation of melanotic nodules. Previously, the silencing of several mitochondrial
510 ribosomal genes in hemocytes has been found to lead to the formation of melanotic nodules in
511 *Drosophila* larvae [48]. Furthermore, Liu et al. [51] observed that ciprofloxacin-fed larvae contained
512 melanised masses. Ciprofloxacin has antimicrobial properties and it is known to interfere with
513 mitochondrial DNA replication and to reduce mtDNA copy number [52]. Moreover, when we
514 inhibited cIII function with antimycin A, we found a dose-specific response in the formation of
515 melanotic nodules and noted that the susceptibility varied between the two fly strains studied. Based
516 on these data, it is reasonable to surmise that tempering with mitochondrial function, either directly
517 by targeting OXPHOS or otherwise reducing mitochondrial performance, is connected with the
518 formation of melanotic nodules in *Drosophila*.

519

520 *Mild mitochondrial perturbations are linked to an increase in circulating hemocytes, hemocyte*
521 *activation and protection against a parasitoid wasp infection*

522 Since melanotic nodules are a common sign of the activation of the fly immune cells, the hemocytes,
523 we next quantified and qualified the hemocytes in our three models. The uninfected mtKSA2 larvae
524 were shown to harbor more hemocytes than the other mitovariants, and the shape analysis of the
525 hemocytes indicated the mtKSA2 larvae have immune-activated hemocyte types, although we could
526 not indisputably verify this. In antimycin A treated larvae, we did not detect signs of hemocyte
527 activation. Of note, we observed that the development of the antimycin A -fed larvae that exhibited
528 melanotic nodules was delayed approximately one day. Since the hemocyte analyses were performed
529 on larvae that reached the late 3rd instar stage at the same rate as the controls (on the 5th day from egg-
530 lay when reared at 29 °C), most antimycin A -fed larvae with visible melanised aggregates were
531 excluded from the analyses. In the case of OXPHOS complex knockdown in hemocytes, the
532 formation of melanotic nodules was indeed associated with the formation of immune-induced
533 hemocyte types, mainly activated plasmatocytes and lamellocytes. Besides the antimycin A -fed
534 larvae, the two other models did not cause a delay in development, indicating that the pharmacological
535 approach and the used consentrations were causing more drastic changes in the animals. This in turn
536 shows that although mild OXPHOS perturbations might be beneficial for the immune response, more
537 severe perturbations are harmful. Indeed, an antimycin A -treatment as well as OXPHOS cI and cV
538 knockdown in the fat body led to a delayed development time and weakend immune response while
539 mitovariant mtKSA2 and OXPHOS gene knockdowns in hemocytes that had no effect on the
540 development time resulted in an enhanced innate immune response. However, when the locomotion
541 activities and sleep patterns were studied in eight *Drosophila* cybrid lines, including those studied
542 here, it was shown that especially the males that had the mitovariant mtKSA2 were moving less and
543 sleeping more than the other cybrids [53]. This indicates that the activated immune system of the
544 mtKSA2 flies might be energetically costly and reflect on the activity levels of the mtKSA2 cybrids.
545

546 *Hemocyte activation in dysfunctional OXPHOS is associated with a loss of mitochondrial membrane*
547 *potential and reduced apoptosis*
548 When studying the silencing of OXPHOS complexes I, III and V in hemocytes in more detail, we
549 found that hemocyte activation was accompanied with, and potentially induced by, the loss of the
550 mitochondrial membrane potential. The mitochondrial membrane potential, the electronic charge
551 difference between the intermembrane space and the mitochondrial matrix, is mainly generated by
552 the action of the proton pumps functioning in OXPHOS (cI, cIII and cIV). We found that in addition
553 to cIII silencing, the membrane potential was reduced also when silencing the ATP synthase stalk
554 subunit *ATPsynCF6* (cV) in hemocytes. The stalk creates the rotation of the membrane embedded F_0
555 domain of the F_1F_0 ATP synthase, thereby enabling the translocation of protons from the
556 intermembrane space to the matrix, where the catalytic F_1 domain facilitates the generation of ATP.
557 This impairment in proton translocation may lead to a reduction in the mitochondrial membrane
558 potential. For example, Bornhövd et al. [54] showed that destabilizing F_1F_0 ATP synthase
559 supracomplex structure led to a loss of membrane potential, possibly via altering the fluidity of the
560 mitochondrial inner membrane. The silencing of the cI gene *ND-75* in hemocytes had a small, and
561 statistically non-significant, effect on the mitochondrial membrane potential, which was reflected on
562 the milder immune response effects in *ND-75* knockdown larvae.
563
564 We also detected a decrease in the amount of apoptotic plasmatocytes when knocking down
565 OXPHOS cIII and cV, but again not cI, in hemocytes. Mitochondria are centrally involved in the
566 control of apoptosis via the release of cytochrome c (cyt c) and several other soluble proteins [55,56],
567 a process requiring the mitochondrial outer membrane permeabilization (MOMP) as a response to
568 various death signals [57]. The production of ROS offers two opposite possibilities for how OXPHOS
569 dysfunction in hemocytes might lead to reduced apoptosis. On the one hand, mild mitochondrial
570 depolarization can reduce the production of mitochondrial ROS (mtROS) and therefore protect the

571 cells from apoptosis induced by excess mtROS [58]. On the other hand, Singh et al. [59] have shown
572 that in myoblasts, dysfunctional electron transfer increased ROS production and created
573 mitohormetic effects protecting the cells from apoptosis. Since we were not able to detect changes in
574 ROS upon OXPHOS silencing in hemocytes, the relation between ROS and apoptosis in this context
575 remains speculative.
576
577 Since apoptosis is an integral part of cellular homeostasis, its dysregulation can be detrimental and
578 involved in pathologies [60]. Ming et al. [61] observed that the hemolymph of apoptosis-deficient
579 *Drosophila* larvae contained damage associated molecular patterns (DAMPs), which led to an
580 inflammatory response including the activation of the Toll signaling. Toll activation in hemocytes
581 and in other tissues, in turn, is known to lead to the formation of melanotic nodules and lamellocytes
582 [62,63]. Noteworthy, apoptosis-defiency has been connected to an increase in necrotic cell death [64],
583 but we did not observe differences in dead or dying hemocytes upon OXPHOS gene knockdown in
584 hemocytes. In addition to a decrease in apoptosis, also an increase in apoptosis has been linked to
585 Toll activation in *Drosophila*: Arefin et al. [65] observed that melanotic nodules and lamellocytes
586 were formed in connection to the activation of Toll signaling when they activated apoptotic pathway
587 in plasmatocytes.
588
589 The observation that *ND-75* (GD strain) knockdown in hemocytes had only a small effect on the
590 mitochondrial membrane potential, a weak melanotic nodule phenotype, virtually no hemocyte
591 activation, and had no effect on the apoptosis, might indicate that the loss of the membrane potential
592 is a crucial component in the immune beneficial phenotypes we observed. The importance of the loss
593 of mitochondrial membrane potential to the immune beneficial effect in hemocytes was further shown
594 with the cII gene *SdhD* knockdown larvae that did not manifest the loss of the membrane potential
595 and also lacked melanotic nodules and hemocyte activation. However, further studies are required to

596 disentangle the possible interplay between the loss of mitochondrial membrane potential and
597 apoptosis in immune activation and lamellocyte formation.
598
599 *ROS is not the ultimate cause of hemocyte activation and an enhanced immune response*
600 As ROS is considered a vital regulatory component of many signalling processes [66–68] and various
601 cellular functions [69–71], we examined if our OXPHOS perturbations affected the production of
602 ROS. We did not observe changes in overall ROS levels in hemocytes when silencing genes encoding
603 for the OXPHOS cI, cIII or cV subunits, but there was an increase in ROS-producing hemocytes in
604 the KSA2 mitovariant when compared to other mitovariants. It must be noted that in our experiments
605 also control hemocytes exhibited high levels of ROS. This may be characteristic to hemocytes, since
606 as immune active cells they may be prone to produce ROS when slightly stressed by dissection and
607 being out of their natural environment. Therefore, we also tested if silencing the expression of
608 antioxidant genes in hemocytes phenocopied the OXPHOS gene silencing phenotypes, namely the
609 formation of melanotic nodules and the enhanced immune response. This was not the case, indicating
610 that ROS is not centrally involved in the beneficial effects seen in an OXPHOS dysfunction immune
611 context, at least not in hemocytes. Noteworthy, in mammals the hematopoietic stem cells (HSC) in
612 the bone marrow rely heavily on glycolysis, and an increase in mitochondrial energy production,
613 accompanied with an increase in ROS production, enables them to go forward with their
614 differentiation program (reviewed in [11]). Similarly, it was shown that in *Drosophila* ROS primes
615 hematopoietic stem cells in the larval hematopoietic organ, the lymph glands, to differentiate into
616 mature hemocytes (crystal cells, plasmatocytes, lamellocytes) [72]. Since silencing the OXPHOS and
617 antioxidant genes in mature hemocytes did not lead to hemocyte differentiation, we conclude that in
618 mature plasmatocytes, ROS is not the driving force in the transdifferentiation into lamellocytes.
619
620

621 *Metabolic changes may accompany enhanced immunity*

622 Understanding how the changes we observed in hemocytes possibly contribute to the activation of
623 immune cells and lamellocyte formation requires further research. However, it is possible that a
624 metabolic switch involving a reduction in OXPHOS activity in plasmatocytes is a trigger launching
625 their activation and transdifferentiation into lamellocytes. Metabolic reprogramming has been shown
626 to be a key event in mammalian immune cell activation, differentiation and function. For example,
627 different T-cell types utilize glycolysis, citric acid cycle and mitochondrial ETC at different levels,
628 but how exactly these changes contribute to T-cell functions is not yet fully understood (reviewed in
629 [73]). Tiwari et al. [74] showed that in the larval hemopoietic organ, the lymph gland, mitochondrial
630 fatty acid β oxidation in progenitor cells is required for hemocyte differentiation, which demonstrates
631 that metabolism acts as a driving force in determining cell indentity also in the fly. Metabolic
632 reprogramming has been shown also in macrophage activation, where pro-inflammatory
633 macrophages increase the activity of aerobic glycolysis and decrease mitochondrial respiration as
634 soon as four hours post exposure to a bacterial-derived lipopolysaccharide [75]. Similarly, *Drosophila*
635 phagocytes, the plasmatocytes, have been shown to switch to aerobic glycolysis when activated upon
636 encountering bacteria [39]. Krejčová et al. [39] found that in the acute phase of a *Streptococcus*
637 *pneumonia* infection hemocytes upregulate the expression of *sima* (HIF-1α) and its target glycolytic
638 genes and exhibit higher glycolytic enzymatic activity. There was also a prominent increase in
639 circulating glucose (the main circulating sugar in adult *Drosophila*) and depleted sugar storages,
640 signifying increased utilization of sugar to fuel aerobicglycolysis. Many of these changes were no
641 longer evident in the resolution phase of the infection, but *Ldh* expression and its enzymatic activity
642 remained at elevated levels compared to uninfected control flies also in a later phase of the infection
643 [39]. We show that mtKSA2 larvae have a tendency towards smaller glycogen reservoirs than the
644 other mitovariants and higher expression of *sima.* In larvae with OXPHOS gene knockdown in
645 hemocytes, we did not find any consistent evidence towards reduced glycogen storages, increased

646 levels of trehalose in the hemolymph or increased *sima* expression. But, we did find that *Ldh*
647 expression was upregulated in *ox* (cIII) and *ATPsynCF6* (cV) knockdown hemocytes. Therefore, it is
648 possible that we captured a "resolution phase" of the effect of OXPHOS gene knockdown in
649 hemocytes and therefore could not detect the earlier signs of the switch to aerobic glycolysis. Since
650 increased *Ldh* expression was seen in samples also containing lamellocytes (*ox* and *ATPsynCF6* KD),
651 this could mean that lamellocytes are expressing *Ldh* at higher levels than plasmatocytes. Indeed,
652 single-cell RNA sequencing of hemocytes has revealed that mature lamellocytes are characterized by
653 a higher expression of glycolytic genes [76], supporting the idea that a switch to glycolysis could
654 initiate the transdifferentiation of plasmatocytes into lamellocytes.
655
656 *Mild mitochondrial dysfunction below a specific threshold can be beneficial for the organism*
657 Overall, the defects in OXPHOS and other mitochondrial functions vary in their severity. The extent
658 of the damage to the organism depends on the type of the defect, the affected tissues, and the possible
659 mutation load [77]. Several studies show how tissue-specific and/or mild mitochondrial dysfunction
660 can benefit the organism. For instance, it was shown that reduced mitochondrial respiratory chain
661 function in muscle cells can lead to protection against increased apoptosis caused by the cholesterol
662 drug statin [59]. Importantly, a recent study showed that treating mice with doxycycline, a drug that
663 affects mitoribosomes and therefore disrupts mitochondrial translation, leads to an increased
664 tolerance of an *Escherichia coli* infection without affecting the pathogen load (resistance) [78]. On
665 the other hand, mitochondrial dysfunction is often harmful, depending not only on the severity but
666 also on the context. Kenny et al. [79] showed that cancer cells with high levels of ROS production
667 and characteristic mitohormetic effects were also more capable to metastasize. In *Drosophila*, it was
668 shown that cybrids with impaired OXPHOS have a higher mortality rate in a *Providencia rettgeri*
669 infection [22]. This effect could result from the mitochondrial translation defect, the severely
670 disrupted mito-nuclear interaction, or both. The same cybrid line was shown to have lower fecundity

671 and embryonic survival of the progeny [80]. These examples show how a severe defect present in the
672 whole organism tends to be harmful, including in the case of infection.
673
674 We show that mild perturbations of OXPHOS both in hemocytes or at an organismal level can be
675 beneficial in the cell-mediated innate immune context and cause variation in infection outcomes.
676 These immune-benefical effects potentially arise from the pre-activation of the immune cells or from
677 a more general retrograde signaling (mitochondria-to-nucleus) event. Further studies are needed to
678 disentangle the mechanisms behind the effects seen in this study. Several factors affect the threshold
679 between beneficial and harmful mitochondrial (dys)functions and make possible applications
680 complex. First, when we silenced OXPHOS complex genes ubiquitously, or in the fat body, a major
681 organ in the larvae, we observed detrimental effects on larval development and eventually pupal
682 lethality in most of the cases. The ability to encapsulate and kill wasps was also impaired upon fat
683 body -specific OXPHOS disruption. Similarly, feeding the cIII inhibitor antimycin A to the larvae
684 hampered the immune response against the parasitoid. This implies that the mitochondrial distruption
685 in these cases was too harsh, and beyond eliciting mitohormetic responses. Second, the studied strains
686 responded differently to the antimycin A doses, showing that dose administration is host-specific
687 when aiming to achieve certain phenotypic, threshold dependent responses. These dose effects also
688 make the therapeutic utiliziation of partial OXPHOS inhibition in infection context somewhat
689 problematic.
690
691 Why individuals respond differently when exposed to the same pathogen remains an intriquing
692 question in immunology. The role of nuclear encoded genes in variable immune responses has been
693 extensively established. Here we show that both mitochondrial functions and mtDNA clearly play an
694 important role in the response to pathogens. We show how simple perturbations to mitochondrial
695 function can result in protective effects that are directly driven by changes in cellular immunity. Our

696 work also underlines how Drosophila model offers powerful means to disentangle variation in
697 immunity that arises from mitochondrial variation and especially from less investigated mtDNA
698 polymorphisms in comparison to variation caused by nuclear genome. Our results therefore
699 contribute to the understanding of innate immunity, by providing information about the genetic causes
700 underlying the variation seen in the response to infections.
701
702 **Materials and methods**
703 ***Cybrid strains***
704 Cytoplasmic hybrid (cybrid) strains were created previously by multiple generations of backcrossing,
705 to obtain fly strains that contain unique mtDNA variants in a controlled Oregon-RT nuclear genome
706 background (ORT; Oregon-R strain maintained in Tampere *Drosophila* laboratory for decades)
707 [4,37]. Prof. Laurie S. Kaguni and Prof. Howard T. Jacobs are thanked for gifting us the cybrid strains.
708 The mtDNA variants mtORT, mtWT5A, mtBS1 and mtKSA2 were chosen from a panel of 10 cybrid
709 strains, based on earlier studies [37]. The mtDNA genome sequences of the chosen mtDNA variants
710 have been published earlier [37]. The amino acid replacement in the protein coding genes and the
711 variation in the tRNA and rRNA genes and the length of the mtDNA of the four mtDNA genomes
712 are summarized in S1 Table.
713
714 ***Targeted gene silencing***
715 The binary GAL4/UAS expression system [81] was utilized for targeted gene silencing using the
716 RNA interference (RNAi) method. RNAi strains for OXPHOS genes, and their respective genetic
717 background w^{1118} strains (called hereafter w^{GD} and w^{KK}) were obtained from the Vienna *Drosophila*
718 Resource Center (VDRC) GD (P-element) and KK (phiC31) RNAi libraries (S2 Table). To express
719 the OXPHOS targeted UAS-RNAi constructs ubiquitously, the *da-GAL4* (Bloomington Drosophila
720 Stock Centre Indiana University, Bloomington, BL #8641) driver was used. For fat body-specific

721 gene silencing, the *FB-GAL4* (*P{GAL4}fat*) driver was used [63,82]. For silencing the gene
722 expression in hemocytes, a combination of two hemocyte GAL4 drivers, the *Hml$^{\Delta}$-GAL4* (BL
723 #30139, [83]) and *He-GAL4.Z* (BL #8699, [84]) was used (*w^{1118}; Hml$^{\Delta}$-GAL4, UAS-2xEGFP; He-*
724 *GAL4, UAS-GFP^{nls}*) and referred to as *Hml$^{\Delta}$-GAL4;He-GAL4.* 20-25 females and 10-13 males of the
725 cybrid lines were used per cross, and the GAL4/UAS crosses were done by crossing 15 virgin GAL4
726 females with 7 UAS-RNAi males.
727
728 ***Fluorescent hemocyte reporter strains***
729 To identify different hemocyte types, *in vivo* hemocyte reporters, the *eater-GFP* (plasmatocytes, [85])
730 and *msnF9mo-mCherry* (lamellocytes, [86]) combined with *Hml$^{\Delta}$-GAL4; He-GAL4* (*yw,msnF9mo-*
731 *mCherry,eater-GFP;Hml$^{\Delta}$-GAL4;He-GAL4*) [34] were utilized. The strain is referred to as *msn-*
732 *mCherry,eater-GFP;Hml$^{\Delta}$-GAL4;He-GAL4.*
733
734 ***Fly maintenance***
735 Flies were reared on a diet containing 36 g of mashed potato powder, 9 g of agar, 45.5 ml corn syrup,
736 14.5 g of dry yeast, 8 g of nipagin and 5g of ascorbic acid per 1 litre of water. All the strains were
737 maintained at 25 °C ± 0.5 °C. Experimental crosses were kept at a 12:12LD cycle at 25°C ± 0.5°C
738 for the first egg laying day and vials with the eggs were either kept at 25 °C ± 0.5 °C or moved to 29
739 °C ± 0.5 °C (60 % humidity), depending on the experiment.
740
741 ***Parasitoid wasp assay***
742 The parasitoid wasp *Leptopilina boulardi* strain G486 was used as a natural model to induce the cell-
743 mediated innate immune response in *Drosophila* larvae. Female flies were allowed to lay eggs for 24
744 hours at +25 °C. The eggs were then either kept at 25 °C or transferred to 29 °C for further
745 development, depending on the experiment. 2nd instar larvae were exposed to 12-15 female wasps for

746 two hours at RT (22 °C), after which the wasps were removed, and the larvae placed back at their
747 rearing temperature. The encapsulation response of the *Drosophila* larvae was checked from 3rd instar
748 larvae, 72 hours after the infection when the larvae were reared at 25 °C and 48 hours post infection
749 at 29 °C, by dissecting the larvae individually in a drop of water under a stereomicroscope. The
750 cellular immune response of the larvae was determined based on their ability to encapsulate and
751 melanise the wasp egg/larva either as i) *no melanisation* (-): the larva failed to encapsulate the wasp
752 egg /larva and the wasp continued its development, ii) *partially melanised* (-/+): the larva was able to
753 elicit the cellular immune response against the wasp larva, which was partially melanised
754 (encapsulated) and *iii) melanised* (+): the wasp larva was completely encapsulated and it was
755 terminated as a sign of a successful cellular immune response. Three replicate crosses per genotype
756 were made, and larvae were dissected until 50 infected larvae per replicate had been collected (150
757 larvae per genotype in total).
758
759 ***Larval glycogen and glucose measurements***
760 Glycogen and glucose were measured using the GAGO-20 kit (Sigma Glucose (GO) assay kit)
761 following the protocol in [87]. Pools of seven 3rd instar larvae per sample (three replicate samples)
762 were used and the sexes were analysed separately. Larvae were homogenized in 100 µl of 1x PBS.
763 To normalize the measurements to the protein content, an aliquot of the sample was taken for
764 measuring the total protein concentration using a BCA assay kit (Merck Millipore). The remaining
765 sample was heat-treated (70 °C, 10 minutes) and centrifuged at 14 000 g and 4 °C for 3 minutes. The
766 supernatant was then diluted 1:5 and pipetted into a 96-well plate in duplicate. The assay was
767 performed according to the GAGO-20 kit protocol. One duplicate was treated with GO reagent only
768 and the other with GO reagent and amyloglucosidase (1 µl of enzyme per 1 ml of GO reagent) to
769 break down glycogen into glucose. A blank (30 µl of 1x PBS), a glucose standard (2-fold serial
770 dilutions from 0.01 to 0.16 mg/ml glucose) and a glycogen standard (2-fold serial dilutions from 0.01

771 to 0.16 mg/ml glycogen) treated with amyloglucosidase were also included. The samples were
772 incubated for 30 minutes at 37°C, and 100 µl of of 12 N sulfuric acid (H2SO4) was added to stop the
773 enzymatic reaction. The absorbance at 540 nm was measured with the a Wallac Envision 2104
774 Multilabel Reader (PerkinElmer). The amount of free glucose was determined from untreated
775 samples using the glucose standard curve. To calculate the amount of glycogen, the absorbance
776 measured for free glucose in the untreated samples was subtracted from the absorbance of the samples
777 treated with amyloglucosidase. The amount of glycogen was then determined from the glycogen
778 standard curve.
779
780 ***Feeding assay***
781 To check whether there was any variation in their food intake/consumption of the larvae, we stained
782 the fly food medium with 0.5 % of Blue FCF dye (Acros Organics A0373695, ThermoFisher
783 Scientific) and reared the larvae on it at 29 °C until they reached the 3rd instar stage. Seven blue food-
784 fed larvae were then pooled per a replicate (sexes separately) and stored at -80 °C prior to the analyses.
785 100 ul of 1 x PBS was added to the frozen larvae, and they were ground. 700 µl of 1 x PBS was added
786 on the samples and they were centrifuged for 3 min at 13 000 g. 200 µl of the aliquot was then used
787 to measure the absorbance at 650 nm with the Wallac Envision 2104 Multilabel Reader as a proxy of
788 the amount of the food in the larval guts.
789
790 ***Cybrid hemocyte analysis***
791 Late 3rd instar larvae were gently washed in a drop of filtered water and individually placed in 20 ul
792 of 1% BSA in 1 x PBS on a 12-well glass plate. The hemolymph was bled out by dissecting the larvae
793 open from one side, along the full length of the larvae. 80 ul of 1% BSA in PBS was added to the
794 sample and a BD Accuri C6 flow cytometer was used to analyse the hemocytes. Each cybrid line was
795 tested on three separate occasions (on different weeks) and each time 10 larvae were dissected per

796 strain. To assess the hemocyte counts, we utilized the fact that hemocytes can be easily separated
797 from other particles based on their location in a forward scatter – side scatter plot ([34], S1A Fig).
798 Dead cells were excluded from the analysis by Propidium iodide (PI) staining (1ul per 100 ul sample)
799 (S2B-B' Fig). Plasmatocytes and crystal cells are small and round in their inactivated state [88] and
800 can be gated using the forward scatter area vs. forward scatter height plot, where they form a
801 population detected at an 45° angle (S2C Fig). This was utilized to separate plasmatocytes and crystal
802 cells from activated immune cells appearing in the circulation after an immune challenge. We
803 specifically aimed to detect lamellocytes, the activated hemocyte type crucial for the encapsulation
804 response against parasitoid wasps. Lamellocytes are irregularly shaped [88], which places them
805 outside of the 45° angle in the forward scatter area *vs.* forward scatter height plot (S2C' Fig). This
806 gating strategy, used also in [89], was further confirmed by using hemocyte reporter lines *eater-GFP*
807 and *msn-mCherry* (S2C-C' Fig). The infection scheme described in the section 2.2 was followed to
808 assess the hemocyte populations from wasp-infected cybrid larvae at two temperatures (25 °C and 29
809 °C).
810
811 ***RNA isolation from larvae***
812 Pools of 10 3rd instar larvae (males and females separately, three replicates per genotype) were
813 collected in Eppendorf tubes, snap frozen and stored at -80 °C. Total RNA was extracted using the
814 TRIzol (Ambion by Life Technologies) method. 125 µl of TRIzol reagent was added to frozen larvae
815 and the tissues were ground using a motor-driven grinder with a fitted pestle. Then, 25 µl of
816 chloroform was added and the samples were vortexed for 20 s, after which they were centrifuged for
817 15 min at 12000 g. The upper phase was pipetted into a new Eppendorf tube, 62.5 µl of isopropanol
818 was added, followed by vortexing for 15 sec and a 10 min incubation at RT. After centrifugation for
819 15 min at 12 000 g, the excess liquid was removed, and the remaining pellet was washed twice with
820 500 ul of 75 % EtOH (centrifuging 5 min at 7500 g). After the second wash, the pellet was air-dried

821 until the EtOH had evaporated, and the pellet was dissolved in 50 µl of nuclease free water. The RNA
822 concentration was determined using a NanoDrop ND-1000 spectrophotometer, and the RNA was
823 diluted to 10 ng/µl prior to storing at -80 °C.
824
825 ***Quantifying ROS in cybrid hemocytes***
826 Pools of 10 male and 10 female late 3rd instar larvae per strain reared at 29 °C were washed 3 times
827 with filtered water and dissected in 250 ul of 1 x Schneider's Drosophila Medium (Gibco) on ice to
828 obtain hemolymph. 500 nM of the CellROX™ green reagent (molecular probes for Life
829 Technologies) diluted in Dimethyl Sulfoxide (DMSO) was added to 250 ul of sample to assess the
830 level of oxidative stress in hemocytes. The CellROX kit is a probe-based system, where the probe is
831 only weakly fluorescent in the reduced state and becomes strongly fluorescent under oxidative
832 conditions. After 1-hour incubation at room temperature in the dark, the samples were immediately
833 analysed using the BD Accuri C6 flow cytometer. Hemocytes were stained with 2.5 µl of Propidium
834 iodide (PI) to exclude dead cells from the analysis. Each cybrid line was tested four times. CellROX
835 green was detected using a 530/33 nm filter and PI using a 610/20 nm filter, excitation was with the
836 488nm laser. 2000 live hemocytes were analysed per sample, each sample contained ~10^4 hemocytes
837 in total. One-color controls (non-fluorescent, PI-only and CellROX-only hemocytes) were used to set
838 the gates (S2A-B Fig). To make sure that we were able to differentiate between different levels of
839 ROS in hemocytes with this method, we run positive (high ROS) and negative (low ROS) controls.
840 In our hands, treating the bled hemocytes with Tert-butyl hydroperoxide (TBHP) as a positive control
841 and with antioxidant N-acetylcysteine (NAC) as a negative control did not produce clear differences
842 in the CellROX signal intensity. Therefore, we used hemocytes from *L. boulardi* -infected larvae as
843 a positive ROS control and larvae fed with NAC (concentration in the food 1mg/ml) starting from
844 the egg lay as a negative control. We were able to confirm that the highest proportion of CellROX-
845 positive hemocytes were found in the untreated wasp-infected larvae, followed by descending

846 CellROX in NAC^- uninfected, NAC^+ infected and finally NAC^+ uninfected larvae. The same was seen
847 when looking at the CellROX intensity in the samples (Supplementary Fig 2C).
848
849 ***Viability assay***
850 Females of the parental crosses were left to lay eggs at 25 °C for two subsequent days, and the vials
851 with eggs were transferred to 29 °C approximately 1 day after the start of the egg lay. The
852 developmental stage of the larvae was checked on the fifth and sixth day after the start of the egg-lay.
853 A final check was done on the eight day after the start of the the egg-lay, when control flies had
854 already eclosed.
855
856 ***Melanotic nodules***
857 3rd instar larvae were individually dissected in a drop of water and the presence of melanotic nodules
858 was inspected using a stereomicroscope. 100 larvae per genotype were checked for the presence of
859 melanotic nodules. Examples of larvae and flies exhibiting melanotic nodules (20 x magnification),
860 and dissected melanotic nodules (40x magnification), were imaged using a Deltapix Invenio 10EIII
861 camera (DeltaPix, Denmark) and Nikon SMZ745T stereomicroscope using the DeltaPix InSight
862 software.
863
864 ***Fluorescent hemocyte reporter analysis***
865 The samples were prepared as described in section "*Cybrid hemocyte analysis".* Each RNAi strain
866 was tested on three separate occasions, and ten larvae were dissected per replicate. Similarly, control
867 larvae were tested for their hemocyte profiles on three separate occasions, and the same control
868 samples were used as a baseline in OXPHOS KD and antioxidant KD experiments. The hemocytes
869 were gated as shown in Supplementary S2A Fig and the hemocytes were classified based on the
870 intensity of the *eater-GFP* and *msn-mCherry* reporters. One-color controls (non-fluorescent, GFP-

871 only and *mCherry*-only hemocytes) were used to set up the gates and to correct fluorescence spill-
872 over to the wrong channel, as described in [34]. GFP was detected using a 510/20 nm filter and
873 mCherry using a 610/20 nm filter, excitation was with the 488nm laser. With this method, five
874 hemocyte populations can be detected, two of which express highly the plasmatocyte reporter *eater-*
875 *GFP* (GFP^{high} and $GFP^{high}mCherry^{low}$), the rest having reduced eater-GFP along with an increase in
876 mCherry expression (GFP^{low}, $GFP^{low}mCherry^{low}$ and $mCherry^{high}$).
877
878 ***Mitochondrial membrane potential***
879 The MitoProbe™ TMRM Assay Kit for Flow Cytometry (Invitrogen) was used to detect changes in
880 the mitochondrial membrane potential ($\Delta\Psi m$) in hemocytes in response to the knockdown of genes
881 of the OXPHOS complex. Hemocytes from 20 male 3rd instar larvae per sample were used for the
882 analysis. The larvae were washed and then dissected in 1x PBS. Samples were stained with 0.4 nM
883 TMRM for 30 minutes, protected from light. The negative control sample was treated with 1 µM
884 carbonyl cyanide m-chlorophenyl hydrazone (CCCP) for 5 minutes prior to the staining to depolarize
885 the mitochondrial membrane. The samples were then analysed using a CytoFlex S flow cytometer
886 (Beckman Coulter). The following channels and gain settings (in parentheses) were used: FSC (20),
887 SSC (40), FITC (to detect GFP, 40), PE (TMRM, 80) and EDC (mCherry, 45). Non-fluorescent
888 hemocytes, and hemocytes expressing/stained with each fluorophore individually were used to
889 calculate the color compensation values and to determine the level of autofluorescence of the
890 hemocytes. $eaterGFP^{high}$ plasmatocytes were used in the analyses to control for the hemocyte type.
891
892 ***Apoptosis***
893 To measure the number of apoptotic cells, we used annexin V staining. During apoptosis,
894 phosphatidylserine is translocated from the inner side of the plasma membrane to the outer side.
895 Annexin V binds to phosphatidylserine, allowing the detection of apoptotic cells using annexin V

896 conjugated to a fluorophore. 20 male 3rd instar larvae per sample were washed and then dissected in
897 100 µl of the annexin-binding buffer (10 mM HEPES, 140 mM NaCl, and 2.5 mM $CaCl_2$, pH 7.4) to
898 release the hemocytes. The samples were kept on ice prior to staining. Then, the samples were stained
899 with 2.5 µl of the Annexin V Pacific Blue conjugate (Invitrogen) and incubated for 15 minutes at RT.
900 After the incubation, the samples were diluted with 400 µl of annexin-binding buffer and analysed
901 using a CytoFlex S flow cytometer. The following channels and gain settings (in parentheses) were
902 used: FSC (20), SSC (40), PB450 (Annexin V Pacific blue, 40), FITC (GFP, 40) and EDC (mCherry,
903 45). Non-fluorescent hemocytes, and hemocytes expressing/stained with each fluorophore
904 individually were used to calculate the color compensation values and to determine the level of
905 autofluorescence of the hemocytes. eaterGFP^{high} plasmatocytes were used in the analyses to control
906 for the hemocyte type.
907
908 ***ROS detection in OXPHOS complex knockdown hemocytes***
909 The CellROX deep red reagent did not work properly in our hands, and so to measure ROS in the
910 hemocytes together with OXPHOS gene knockdown, the CellROX green probe was utilized as
911 described in section 2.10. Male flies of the OXPHOS complex knockdown strain were crossed with
912 a version of the hemocyte reporter without the *UAS-GFP^{nls}* constructs (*w^{1118};+;Hml$^{\Delta}$-GAL4,He-*
913 *GAL4*). The hemocytes were analysed with a CytoFlex S flow cytometer with the following settings:
914 FSC (20), SSC (40), FITC (40) and PC5.5 (PI, 170).
915
916 ***Glucose and trehalose measurements from larval hemolymph***
917 Pools of 20 larvae (sexes separated) were washed carefully in filtered water with a brush to remove
918 any food particles. Larvae were pricked using stainless steel Austerlitz insect pins of 0.2 mm in
919 diameter (Entomoravia), horizontally from the posterior end towards the anterior end, avoiding
920 damaging the gut. Pricked larvae were collected in a 100 µm pluriStrainer mini 100 filter placed in a

921 1.5 ml Eppendorf tube on ice. The samples were centrifuged for 7 min at 5000 g at 4 °C and 1 µl of
922 hemolymph was collected. 1 µl of hemolymph was then mixed with 99 µl of trehalase buffer (TB, 5
923 mM Tris pH 6.6, 137 mM NaCl, 2.7 mM KCl). 25 µl aliquots of samples were snap-frozen and stored
924 for a protein concentration measurement. After heat-inactivating the samples (70 °C, 5 min), each
925 sample was divided in two aliquots, and 3 µl of Porcine kidney trehalase (Sigma) was added to one
926 of the aliquots to break down trehalose into glucose. After an overnight incubation with the enzyme,
927 30 µl of a blank (1 x PBS), a glucose standard (2-fold serial dilutions from 0.01 to 0.16 mg/ml
928 glucose) and duplicates of the samples were pipetted into a 96-well plate and the assay was then
929 performed according to the GAGO-20 kit protocol as described above. The absorbance at 540 nm
930 was measured with a Wallac Envision 2104 Multilabel Reader. The amount of free glucose in the
931 untreated samples was determined with the help of the glucose standard curve. The amount of
932 trehalose was calculated by first subtracting the absorbance of free glucose from the samples treated
933 with trehalase, and then using the trehalose standard curve to calculate the trehalose concentration.
934
935 ***Hemocyte RNA isolation***
936 3rd instar larvae were dissected in ice cold 1 x PBS on a 12-well glass slide to release the hemolymph.
937 The hemolymph from 50 larvae (males and females separately) was pooled per sample (three replicate
938 samples per genotype) and centrifuged for 7 minutes at 2500 g at 4 °C to pellet the hemocytes. As
939 much of the PBS was removed as possible (the hemocyte pellet is not visible and is loosely attached
940 on the Eppendorf tube) prior to storing the samples at -80 °C. Total RNA was extracted with the
941 Single Cell RNA Purification Kit (Norgen Biotek) protocol that is optimized for extracting RNA from
942 low numbers of cells. Samples were treated with DNase I (RNAse free DNase I kit, Norgen Biotek)
943 as described in the manufacturer's protocol. The RNA quality was checked using a NanoDrop ND-
944 1000 spectrophotometer (Thermo Scientific) and each sample was diluted to 10 ng/µl prior to storing
945 at -80 °C.

946 ***Gene expression***

947 Quantitative Real-time PCR (qRT-PCR) was used to detect the expression levels of the genes of
948 interest (from hemocytes or whole larvae) and to quantify the efficiency of OXPHOS gene
949 knockdown in the larval hemocytes. For the qRT-PCR reactions, the iTaq Universal Sybr green One-
950 step kit (Bio-Rad) was used. 10 µl reaction mix per sample was as follows: 5 µl of iTaq universal
951 SYBR Green reaction mix (2x), 0.125 µl of iScript reverse transcriptase (RT), 0.3 µl of forward and
952 reverse primers each (300 nM each), 2 µl of template RNA (20 ng per reaction) and 2.275 µl of
953 nuclease free H_2O. Each plate run included a sample without RT and a sample without an RNA
954 template for quality checking. The samples were run with a Bio-Rad CFX96 Real-time PCR system
955 with a reverse transcription reaction for 10 min at 50 °C, polymerase activation and DNA denaturation
956 for 1 min at 95 °C followed by 39 cycles of amplification (denaturation for 10 sec at 95 °C,
957 annealing/extension for 15 sec at 60 °C) and a melt-curve analysis at 65-95 °C in 0.5 °C increments.
958 The efficiency of each primer pair was calculated, and a primer pair was deemed usable, if the
959 efficiency fell between 90-110%. The efficiencies were calculated based on the slope of the
960 regression line obtained from a 5-fold serial dilution of the template RNA (each point assayed in
961 duplicate), using the following formula: Efficiency (%) = $(-1/10^{slope} – 1) \times 100$ built into the Bio-Rad
962 software. Primers and their efficiencies are shown in S4 Table. The average threshold cycle (Ct)
963 values were calculated from two technical replicates per three biological replicates. For the cybrids,
964 gene expression was calculated as $2^{\Delta Ct}$, and for the OXPHOS RNAi strains, relative expression was
965 calculated as $2^{\Delta\Delta Ct}$, using the genetic background strain crossed with the driver strain as a control
966 treatment. In all analyses, *Histone H3.3b* (*His3.3b*) was used as a reference gene.

967

968 ***Antimycin A treatment***

969 Concentrations of 4, 6 and 8 ug/mL of antimycin A (Enzo Life Sciences) in the fly food medium were
970 chosen based on earlier studies [23]. The nuclear background strain of the cybrids ORT and the

971 background strain of the RNAi (GD library) lines w^{GD} were used in the antimycin A assays. 25-30
972 females and 10 males of the strains ORT and w^{GD} were mated, and the females were left to lay eggs
973 at 25 °C in regular food. After two days the late 1st- early 2nd instar larvae were transferred to food
974 vials containing antimycin A and placed at 29 °C. This was repeated several times to obtain enough
975 larvae for the assays. 100 3rd instar larvae were dissected from ORT and w^{GD} strains reared on the
976 three antimycin A concentrations to check for the presence of melanotic nodules. The effect on the
977 response against *L. boulardi* parasitoid wasps (n=100) and on hemocyte composition (n=30) were
978 studied using 3rd instar w^{GD} larvae fed with 6 ug/ml antimycin A. In addition, the hemocyte
979 composition was assessed from 3rd instar hemocyte reporter larvae (*msn-mCherry,eater-GFP;Hml*$^{\Delta}$-
980 *GAL4;He-GAL4/*w^{GD}) reared on 6 ug/ml antimycin A food at 29 °C to gain a more detailed picture
981 of the effect of antimycin A on hemocyte profiles.
982
983 ***Statistical analyses***
984 R version 4.0.4 and Excel version 16.60 (Microsoft) were used for analysing the data and R was used
985 for plotting. The data on proportions (wasp assay, apoptotic cells, ROS-positive cells) were analysed
986 using logistic regression with a binomial distribution with the lm4 package [90]. In the case of the
987 immune response against wasps, non-melanised and partially melanised cases were deemed as a
988 failure and fully melanised as a success. When needed, pairwise comparisions of the strains were
989 analysed using the multcomp package [91]. The data on cell counts were analysed using a generalized
990 linear model with negative binomial distribution using the MASS package [92]. The least square
991 means (estimated marginal means) were analysed for multiple comparisons among the strains and the
992 Tukey method was used for adjusting the p-value using the emmeans package [93]. Data on feeding
993 rates, trehalose and glycogen consentrations and gene expression were analysed using Kruskall-
994 Wallis tests followed by a pairwise student's t-tests or the Wilcox tests.
995

Acknowledgements

We thank Angelika Pölläniemi (Tampere University) for technical assistance and Tilman Tietz for commenting the manuscript. Resources for fly work were provided by Tampere Drosophila Core Facility. The Tampere facility of Flow Cytometry is acknowledged for their services. Financial support was provided by the Academy of Finland (322732 and 328979) and the Sigrid Jusélius foundation (3122800849) grants to TSS, Tampere University Doctoral School funding to YB and a Leverhulme Trust Research Project grant (RPG-2018-369) and a Branco Weiss Fellowship to PV. The funders had no role in study design, data collection and analysis, decision to publish, or preparation of the manuscript.

Author contributions

LV – original draft, data analysis, result figures, supervision, experimental work, review and editing. YB – original draft, experimental work, data analysis, result figures. TT – experimental work. PV – review and editing, funding acquisition. TSS – original idea, original draft, funding acquisition, supervision, project administration, review and editing, experimental work.

Competing interests

The authors have declared no competing interest.

1021 **References**

1022 [1] Breda CN de S, Davanzo GG, Basso PJ, Saraiva Câmara NO, Moraes-Vieira PMM.
1023 Mitochondria as central hub of the immune system. Redox Biol 2019;26:101255.
1024 https://doi.org/10.1016/j.redox.2019.101255.
1025 [2] Mills EL, Kelly B, O'Neill LAJ. Mitochondria are the powerhouses of immunity. Nat
1026 Immunol 2017;18:488–98. https://doi.org/10.1038/ni.3704.
1027 [3] Mohanty A, Tiwari-Pandey R, Pandey NR. Mitochondria: the indispensable players in
1028 innate immunity and guardians of the inflammatory response. J Cell Commun Signal 2019;13:303–
1029 18. https://doi.org/10.1007/s12079-019-00507-9.
1030 [4] Salminen TS, Vale PF. Drosophila as a Model System to Investigate the Effects of
1031 Mitochondrial Variation on Innate Immunity. Front Immunol 2020;11:521.
1032 https://doi.org/10.3389/fimmu.2020.00521.
1033 [5] Shekhova E. Mitochondrial reactive oxygen species as major effectors of
1034 antimicrobial immunity. PLOS Pathog 2020;16:e1008470.
1035 https://doi.org/10.1371/journal.ppat.1008470.
1036 [6] Tiku V, Tan M-W, Dikic I. Mitochondrial Functions in Infection and Immunity.
1037 Trends Cell Biol 2020;30:263–75. https://doi.org/10.1016/j.tcb.2020.01.006.
1038 [7] Bailis W, Shyer JA, Zhao J, Canaveras JCG, Al Khazal FJ, Qu R, et al. Distinct
1039 modes of mitochondrial metabolism uncouple T cell differentiation and function. Nature
1040 2019;571:403–7. https://doi.org/10.1038/s41586-019-1311-3.
1041 [8] Suzuki H, Hisamatsu T, Chiba S, Mori K, Kitazume MT, Shimamura K, et al.
1042 Glycolytic pathway affects differentiation of human monocytes to regulatory macrophages.
1043 Immunol Lett 2016;176:18–27. https://doi.org/10.1016/j.imlet.2016.05.009.
1044 [9] Bantug GR, Galluzzi L, Kroemer G, Hess C. The spectrum of T cell metabolism in
1045 health and disease. Nat Rev Immunol 2018;18:19–34. https://doi.org/10.1038/nri.2017.99.
1046 [10] Biswas SK, Mantovani A. Orchestration of Metabolism by Macrophages. Cell Metab
1047 2012;15:432–7. https://doi.org/10.1016/j.cmet.2011.11.013.
1048 [11] Papa L, Djedaini M, Hoffman R. Mitochondrial Role in Stemness and Differentiation
1049 of Hematopoietic Stem Cells. Stem Cells Int 2019;2019:1–10.
1050 https://doi.org/10.1155/2019/4067162.
1051 [12] Marelli-Berg FM, Fu H, Mauro C. Molecular mechanisms of metabolic
1052 reprogramming in proliferating cells: implications for T-cell-mediated immunity: The metabolic
1053 control of T-cell immunity. Immunology 2012;136:363–9. https://doi.org/10.1111/j.1365-
1054 2567.2012.03583.x.
1055 [13] Viola A, Munari F, Sánchez-Rodríguez R, Scolaro T, Castegna A. The Metabolic
1056 Signature of Macrophage Responses. Front Immunol 2019;10:1462.
1057 https://doi.org/10.3389/fimmu.2019.01462.
1058 [14] Warburg O. On the Origin of Cancer Cells. Science 1956;123:309–14.
1059 https://doi.org/10.1126/science.123.3191.309.
1060 [15] Dowling D, Friberg U, Lindell J. Evolutionary implications of non-neutral
1061 mitochondrial genetic variation. Trends Ecol Evol 2008;23:546–54.
1062 https://doi.org/10.1016/j.tree.2008.05.011.
1063 [16] Yonova-Doing E, Calabrese C, Gomez-Duran A, Schon K, Wei W, Karthikeyan S, et
1064 al. An atlas of mitochondrial DNA genotype–phenotype associations in the UK Biobank. Nat Genet
1065 2021;53:982–93. https://doi.org/10.1038/s41588-021-00868-1.
1066 [17] Yu X, Gimsa U, Wester-Rosenlöf L, Kanitz E, Otten W, Kunz M, et al. Dissecting the
1067 effects of mtDNA variations on complex traits using mouse conplastic strains. Genome Res
1068 2009;19:159–65. https://doi.org/10.1101/gr.078865.108.
1069 [18] Zhu Z, Lu Q, Zeng F, Wang J, Huang S. Compatibility between mitochondrial and

1070 nuclear genomes correlates with the quantitative trait of lifespan in Caenorhabditis elegans. Sci Rep
1071 2015;5:17303. https://doi.org/10.1038/srep17303.
1072 [19] Gorman GS, Schaefer AM, Ng Y, Gomez N, Blakely EL, Alston CL, et al. Prevalence
1073 of nuclear and mitochondrial DNA mutations related to adult mitochondrial disease. Ann Neurol
1074 2015;77:753–9. https://doi.org/10.1002/ana.24362.
1075 [20] Pacheu-Grau D, Rucktaeschel R, Deckers M. Mitochondrial dysfunction and its role
1076 in tissue-specific cellular stress. Cell Stress 2018;2:184–99.
1077 https://doi.org/10.15698/cst2018.07.147.
1078 [21] Kapnick SM, Pacheco SE, McGuire PJ. The emerging role of immune dysfunction in
1079 mitochondrial diseases as a paradigm for understanding immunometabolism. Metabolism
1080 2018;81:97–112. https://doi.org/10.1016/j.metabol.2017.11.010.
1081 [22] Buchanan JL, Meiklejohn CD, Montooth KL. Mitochondrial Dysfunction and
1082 Infection Generate Immunity–Fecundity Tradeoffs in Drosophila. Integr Comp Biol 2018;58:591–
1083 603. https://doi.org/10.1093/icb/icy078.
1084 [23] Salminen TS, Cannino G, Oliveira MT, Lillsunde P, Jacobs HT, Kaguni LS. Lethal
1085 Interaction of Nuclear and Mitochondrial Genotypes in *Drosophila melanogaster*. G3
1086 GenesGenomesGenetics 2019;9:2225–34. https://doi.org/10.1534/g3.119.400315.
1087 [24] Minakhina S, Steward R. Melanotic Mutants in Drosophila: Pathways and
1088 Phenotypes. Genetics 2006;174:253–63. https://doi.org/10.1534/genetics.106.061978.
1089 [25] Yun J, Finkel T. Mitohormesis. Cell Metab 2014;19:757–66.
1090 https://doi.org/10.1016/j.cmet.2014.01.011.
1091 [26] Buchon N, Silverman N, Cherry S. Immunity in Drosophila melanogaster — from
1092 microbial recognition to whole-organism physiology. Nat Rev Immunol 2014;14:796–810.
1093 https://doi.org/10.1038/nri3763.
1094 [27] Holz A, Bossinger B, Strasser T, Janning W, Klapper R. The two origins of
1095 hemocytes in *Drosophila*. Development 2003;130:4955–62. https://doi.org/10.1242/dev.00702.
1096 [28] Weavers H, Wood W. Creating a Buzz about Macrophages: The Fly as an In Vivo
1097 Model for Studying Immune Cell Behavior. Dev Cell 2016;38:129–32.
1098 https://doi.org/10.1016/j.devcel.2016.07.002.
1099 [29] Rizki MTM. Alterations in the haemocyte population of Drosophila melanogaster. J
1100 Morphol 1957;100:437–58. https://doi.org/10.1002/jmor.1051000303.
1101 [30] Wang L, Kounatidis I, Ligoxygakis P. Drosophila as a model to study the role of
1102 blood cells in inflammation, innate immunity and cancer. Front Cell Infect Microbiol 2014;3.
1103 https://doi.org/10.3389/fcimb.2013.00113.
1104 [31] Galko MJ, Krasnow MA. Cellular and Genetic Analysis of Wound Healing in
1105 Drosophila Larvae. PLoS Biol 2004;2:e239. https://doi.org/10.1371/journal.pbio.0020239.
1106 [32] Leitão AB, Sucena É. Drosophila sessile hemocyte clusters are true hematopoietic
1107 tissues that regulate larval blood cell differentiation. ELife 2015;4:e06166.
1108 https://doi.org/10.7554/eLife.06166.
1109 [33] Krzemien J, Oyallon J, Crozatier M, Vincent A. Hematopoietic progenitors and
1110 hemocyte lineages in the Drosophila lymph gland. Dev Biol 2010;346:310–9.
1111 https://doi.org/10.1016/j.ydbio.2010.08.003.
1112 [34] Anderl I, Vesala L, Ihalainen TO, Vanha-aho L-M, Andó I, Rämet M, et al.
1113 Transdifferentiation and Proliferation in Two Distinct Hemocyte Lineages in Drosophila
1114 melanogaster Larvae after Wasp Infection. PLOS Pathog 2016;12:e1005746.
1115 https://doi.org/10.1371/journal.ppat.1005746.
1116 [35] Márkus R, Laurinyecz B, Kurucz É, Honti V, Bajusz I, Sipos B, et al. Sessile
1117 hemocytes as a hematopoietic compartment in *Drosophila melanogaster*. Proc Natl Acad Sci
1118 2009;106:4805–9. https://doi.org/10.1073/pnas.0801766106.
1119 [36] Stofanko M, Kwon SY, Badenhorst P. Lineage Tracing of Lamellocytes Demonstrates

1120 Drosophila Macrophage Plasticity. PLoS ONE 2010;5:e14051.
1121 https://doi.org/10.1371/journal.pone.0014051.
1122 [37] Salminen TS, Oliveira MT, Cannino G, Lillsunde P, Jacobs HT, Kaguni LS.
1123 Mitochondrial genotype modulates mtDNA copy number and organismal phenotype in Drosophila.
1124 Mitochondrion 2017;34:75–83. https://doi.org/10.1016/j.mito.2017.02.001.
1125 [38] Hudry B, de Goeij E, Mineo A, Gaspar P, Hadjieconomou D, Studd C, et al. Sex
1126 Differences in Intestinal Carbohydrate Metabolism Promote Food Intake and Sperm Maturation.
1127 Cell 2019;178:901-918.e16. https://doi.org/10.1016/j.cell.2019.07.029.
1128 [39] Krejčová G, Danielová A, Nedbalová P, Kazek M, Strych L, Chawla G, et al.
1129 Drosophila macrophages switch to aerobic glycolysis to mount effective antibacterial defense.
1130 ELife 2019;8:e50414. https://doi.org/10.7554/eLife.50414.
1131 [40] Dudzic JP, Kondo S, Ueda R, Bergman CM, Lemaitre B. Drosophila innate immunity:
1132 regional and functional specialization of prophenoloxidases. BMC Biol 2015;13:81.
1133 https://doi.org/10.1186/s12915-015-0193-6.
1134 [41] Zhao R, Jiang S, Zhang L, Yu Z. Mitochondrial electron transport chain, ROS
1135 generation and uncoupling (Review). Int J Mol Med 2019. https://doi.org/10.3892/ijmm.2019.4188.
1136 [42] Celotto AM, Liu Z, VanDemark AP, Palladino MJ. A novel *Drosophila* SOD 2
1137 mutant demonstrates a role for mitochondrial ROS in neurodevelopment and disease. Brain Behav
1138 2012;2:424–34. https://doi.org/10.1002/brb3.73.
1139 [43] Missirlis F, Hu J, Kirby K, Hilliker AJ, Rouault TA, Phillips JP. Compartment-
1140 specific Protection of Iron-Sulfur Proteins by Superoxide Dismutase. J Biol Chem
1141 2003;278:47365–9. https://doi.org/10.1074/jbc.M307700200.
1142 [44] Kwong LK, Mockett RJ, Bayne A-CV, Orr WC, Sohal RS. Decreased Mitochondrial
1143 Hydrogen Peroxide Release in Transgenic Drosophila melanogaster Expressing Intramitochondrial
1144 Catalase. Arch Biochem Biophys 2000;383:303–8. https://doi.org/10.1006/abbi.2000.2093.
1145 [45] Brodin P, Davis MM. Human immune system variation. Nat Rev Immunol
1146 2017;17:21–9. https://doi.org/10.1038/nri.2016.125.
1147 [46] Feehan J, Tripodi N, Apostolopoulos V. The twilight of the immune system: The
1148 impact of immunosenescence in aging. Maturitas 2021;147:7–13.
1149 https://doi.org/10.1016/j.maturitas.2021.02.006.
1150 [47] Klein SL, Flanagan KL. Sex differences in immune responses. Nat Rev Immunol
1151 2016;16:626–38. https://doi.org/10.1038/nri.2016.90.
1152 [48] Avet-Rochex A, Boyer K, Polesello C, Gobert V, Osman D, Roch F, et al. An in vivo
1153 RNA interference screen identifies gene networks controlling Drosophila melanogasterblood cell
1154 homeostasis. BMC Dev Biol 2010;10:65. https://doi.org/10.1186/1471-213X-10-65.
1155 [49] Ekas LA, Cardozo TJ, Flaherty MS, McMillan EA, Gonsalves FC, Bach EA.
1156 Characterization of a dominant-active STAT that promotes tumorigenesis in Drosophila. Dev Biol
1157 2010;344:621–36. https://doi.org/10.1016/j.ydbio.2010.05.497.
1158 [50] Kim MJ, Choe K-M. Basement Membrane and Cell Integrity of Self-Tissues in
1159 Maintaining Drosophila Immunological Tolerance. PLoS Genet 2014;10:e1004683.
1160 https://doi.org/10.1371/journal.pgen.1004683.
1161 [51] Liu J, Li X, Wang X. Toxicological effects of ciprofloxacin exposure to Drosophila
1162 melanogaster. Chemosphere 2019;237:124542. https://doi.org/10.1016/j.chemosphere.2019.124542.
1163 [52] Hangas A, Aasumets K, Kekäläinen NJ, Paloheinä M, Pohjoismäki JL, Gerhold JM, et
1164 al. Ciprofloxacin impairs mitochondrial DNA replication initiation through inhibition of
1165 Topoisomerase 2. Nucleic Acids Res 2018;46:9625–36. https://doi.org/10.1093/nar/gky793.
1166 [53] Anderson L, Camus MF, Monteith KM, Salminen TS, Vale PF. Variation in
1167 mitochondrial DNA affects locomotor activity and sleep in Drosophila melanogaster. Heredity
1168 2022. https://doi.org/10.1038/s41437-022-00554-w.
1169 [54] Bornhövd C, Vogel F, Neupert W, Reichert AS. Mitochondrial Membrane Potential Is

1170 Dependent on the Oligomeric State of F1F0-ATP Synthase Supracomplexes. J Biol Chem
1171 2006;281:13990–8. https://doi.org/10.1074/jbc.M512334200.
1172 [55] Ott M, Robertson JD, Gogvadze V, Zhivotovsky B, Orrenius S. Cytochrome *c* release
1173 from mitochondria proceeds by a two-step process. Proc Natl Acad Sci 2002;99:1259–63.
1174 https://doi.org/10.1073/pnas.241655498.
1175 [56] Zou H, Li Y, Liu X, Wang X. An APAF-1·Cytochrome c Multimeric Complex Is a
1176 Functional Apoptosome That Activates Procaspase-9. J Biol Chem 1999;274:11549–56.
1177 https://doi.org/10.1074/jbc.274.17.11549.
1178 [57] Dadsena S, Jenner A, García-Sáez AJ. Mitochondrial outer membrane
1179 permeabilization at the single molecule level. Cell Mol Life Sci 2021;78:3777–90.
1180 https://doi.org/10.1007/s00018-021-03771-4.
1181 [58] Vyssokikh MY, Holtze S, Averina OA, Lyamzaev KG, Panteleeva AA, Marey MV, et
1182 al. Mild depolarization of the inner mitochondrial membrane is a crucial component of an anti-
1183 aging program. Proc Natl Acad Sci 2020;117:6491–501. https://doi.org/10.1073/pnas.1916414117.
1184 [59] Singh F, Charles A-L, Schlagowski A-I, Bouitbir J, Bonifacio A, Piquard F, et al.
1185 Reductive stress impairs myoblasts mitochondrial function and triggers mitochondrial hormesis.
1186 Biochim Biophys Acta BBA - Mol Cell Res 2015;1853:1574–85.
1187 https://doi.org/10.1016/j.bbamcr.2015.03.006.
1188 [60] Singh R, Letai A, Sarosiek K. Regulation of apoptosis in health and disease: the
1189 balancing act of BCL-2 family proteins. Nat Rev Mol Cell Biol 2019;20:175–93.
1190 https://doi.org/10.1038/s41580-018-0089-8.
1191 [61] Ming M, Obata F, Kuranaga E, Miura M. Persephone/Spätzle Pathogen Sensors
1192 Mediate the Activation of Toll Receptor Signaling in Response to Endogenous Danger Signals in
1193 Apoptosis-deficient Drosophila. J Biol Chem 2014;289:7558–68.
1194 https://doi.org/10.1074/jbc.M113.543884.
1195 [62] Lemaitre B, Meister M, Govind S, Georgel P, Steward R, Reichhart JM, et al.
1196 Functional analysis and regulation of nuclear import of dorsal during the immune response in
1197 Drosophila. EMBO J 1995;14:536–45. https://doi.org/10.1002/j.1460-2075.1995.tb07029.x.
1198 [63] Schmid MR, Anderl I, Vesala L, Vanha-aho L-M, Deng X-J, Rämet M, et al. Control
1199 of Drosophila Blood Cell Activation via Toll Signaling in the Fat Body. PLoS ONE
1200 2014;9:e102568. https://doi.org/10.1371/journal.pone.0102568.
1201 [64] Silva MT, do Vale A, dos Santos NMN. Secondary necrosis in multicellular animals:
1202 an outcome of apoptosis with pathogenic implications. Apoptosis 2008;13:463–82.
1203 https://doi.org/10.1007/s10495-008-0187-8.
1204 [65] Arefin B, Kucerova L, Krautz R, Kranenburg H, Parvin F, Theopold U. Apoptosis in
1205 Hemocytes Induces a Shift in Effector Mechanisms in the Drosophila Immune System and Leads to
1206 a Pro-Inflammatory State. PLOS ONE 2015;10:e0136593.
1207 https://doi.org/10.1371/journal.pone.0136593.
1208 [66] Murphy MP, Holmgren A, Larsson N-G, Halliwell B, Chang CJ, Kalyanaraman B, et
1209 al. Unraveling the Biological Roles of Reactive Oxygen Species. Cell Metab 2011;13:361–6.
1210 https://doi.org/10.1016/j.cmet.2011.03.010.
1211 [67] Pinegin B, Vorobjeva N, Pashenkov M, Chernyak B. The role of mitochondrial ROS
1212 in antibacterial immunity. J Cell Physiol 2018;233:3745–54. https://doi.org/10.1002/jcp.26117.
1213 [68] Reczek CR, Chandel NS. ROS-dependent signal transduction. Curr Opin Cell Biol
1214 2015;33:8–13. https://doi.org/10.1016/j.ceb.2014.09.010.
1215 [69] Liochev SI. Reactive oxygen species and the free radical theory of aging. Free Radic
1216 Biol Med 2013;60:1–4. https://doi.org/10.1016/j.freeradbiomed.2013.02.011.
1217 [70] Powers SK, Duarte J, Kavazis AN, Talbert EE. Reactive oxygen species are signalling
1218 molecules for skeletal muscle adaptation: Redox signalling and skeletal muscle. Exp Physiol
1219 2010;95:1–9. https://doi.org/10.1113/expphysiol.2009.050526.

1220 [71] Ray PD, Huang B-W, Tsuji Y. Reactive oxygen species (ROS) homeostasis and redox
1221 regulation in cellular signaling. Cell Signal 2012;24:981–90.
1222 https://doi.org/10.1016/j.cellsig.2012.01.008.
1223 [72] Owusu-Ansah E, Banerjee U. Reactive oxygen species prime Drosophila
1224 haematopoietic progenitors for differentiation. Nature 2009;461:537–41.
1225 https://doi.org/10.1038/nature08313.
1226 [73] Steinert EM, Vasan K, Chandel NS. Mitochondrial Metabolism Regulation of T Cell–
1227 Mediated Immunity. Annu Rev Immunol 2021;39:395–416. https://doi.org/10.1146/annurev-
1228 immunol-101819-082015.
1229 [74] Tiwari SK, Toshniwal AG, Mandal S, Mandal L. Fatty acid β-oxidation is required for
1230 the differentiation of larval hematopoietic progenitors in Drosophila. ELife 2020;9:e53247.
1231 https://doi.org/10.7554/eLife.53247.
1232 [75] Haschemi A, Kosma P, Gille L, Evans CR, Burant CF, Starkl P, et al. The
1233 Sedoheptulose Kinase CARKL Directs Macrophage Polarization through Control of Glucose
1234 Metabolism. Cell Metab 2012;15:813–26. https://doi.org/10.1016/j.cmet.2012.04.023.
1235 [76] Cattenoz PB, Sakr R, Pavlidaki A, Delaporte C, Riba A, Molina N, et al. Temporal
1236 specificity and heterogeneity of *Drosophila* immune cells. EMBO J 2020;39.
1237 https://doi.org/10.15252/embj.2020104486.
1238 [77] Tuppen HAL, Blakely EL, Turnbull DM, Taylor RW. Mitochondrial DNA mutations
1239 and human disease. Biochim Biophys Acta BBA - Bioenerg 2010;1797:113–28.
1240 https://doi.org/10.1016/j.bbabio.2009.09.005.
1241 [78] Colaço HG, Barros A, Neves-Costa A, Seixas E, Pedroso D, Velho T, et al.
1242 Tetracycline Antibiotics Induce Host-Dependent Disease Tolerance to Infection. Immunity
1243 2020:S1074761320304052. https://doi.org/10.1016/j.immuni.2020.09.011.
1244 [79] Kenny TC, Craig AJ, Villanueva A, Germain D. Mitohormesis Primes Tumor
1245 Invasion and Metastasis. Cell Rep 2019;27:2292-2303.e6.
1246 https://doi.org/10.1016/j.celrep.2019.04.095.
1247 [80] Zhang C, Montooth KL, Calvi BR. Incompatibility between mitochondrial and
1248 nuclear genomes during oogenesis results in ovarian failure and embryonic lethality. Development
1249 2017:dev.151951. https://doi.org/10.1242/dev.151951.
1250 [81] Brand AH, Perrimon N. Targeted gene expression as a means of altering cell fates and
1251 generating dominant phenotypes. Dev Camb Engl 1993;118:401–15.
1252 [82] Grönke S, Beller M, Fellert S, Ramakrishnan H, Jäckle H, Kühnlein RP. Control of
1253 Fat Storage by a Drosophila PAT Domain Protein. Curr Biol 2003;13:603–6.
1254 https://doi.org/10.1016/S0960-9822(03)00175-1.
1255 [83] Sinenko SA, Mathey-Prevot B. Increased expression of Drosophila tetraspanin,
1256 Tsp68C, suppresses the abnormal proliferation of ytr-deficient and Ras/Raf-activated hemocytes.
1257 Oncogene 2004;23:9120–8. https://doi.org/10.1038/sj.onc.1208156.
1258 [84] Zettervall C-J, Anderl I, Williams MJ, Palmer R, Kurucz E, Ando I, et al. A directed
1259 screen for genes involved in Drosophila blood cell activation. Proc Natl Acad Sci 2004;101:14192–
1260 7. https://doi.org/10.1073/pnas.0403789101.
1261 [85] Sorrentino RP, Tokusumi T, Schulz RA. The Friend of GATA protein U-shaped
1262 functions as a hematopoietic tumor suppressor in Drosophila. Dev Biol 2007;311:311–23.
1263 https://doi.org/10.1016/j.ydbio.2007.08.011.
1264 [86] Tokusumi T, Sorrentino RP, Russell M, Ferrarese R, Govind S, Schulz RA.
1265 Characterization of a Lamellocyte Transcriptional Enhancer Located within the misshapen Gene of
1266 Drosophila melanogaster. PLoS ONE 2009;4:e6429. https://doi.org/10.1371/journal.pone.0006429.
1267 [87] Tennessen JM, Barry WE, Cox J, Thummel CS. Methods for studying metabolism in
1268 Drosophila. Methods 2014;68:105–15. https://doi.org/10.1016/j.ymeth.2014.02.034.
1269 [88] Rizki TM, Rizki RM. The Cellular Defense System of Drosophila melanogaster. In:

King RC, Akai H, editors. Insect Ultrastruct., Boston, MA: Springer US; 1984, p. 579–604. https://doi.org/10.1007/978-1-4613-2715-8_16.

[89] Järvelä-Stölting M, Vesala L, Maasdorp MK, Ciantar J, Rämet M, Valanne S. Proteasome α6 Subunit Negatively Regulates the JAK/STAT Pathway and Blood Cell Activation in Drosophila melanogaster. Front Immunol 2021;12:729631. https://doi.org/10.3389/fimmu.2021.729631.

[90] Bates D, Mächler M, Bolker B, Walker S. Fitting Linear Mixed-Effects Models Using **lme4**. J Stat Softw 2015;67. https://doi.org/10.18637/jss.v067.i01.

[91] Hothorn T, Bretz F, Westfall P. Simultaneous Inference in General Parametric Models. Biom J 2008;50:346–63. https://doi.org/10.1002/bimj.200810425.

[92] Venables WN, Ripley BD. Modern applied statistics with S. 4th ed. New York: Springer; 2002.

[93] Lenth RV. emmeans: Estimated Marginal Means, aka Least-Squares Means. R package version 1.7.3. https://CRAN.R-project.org/package=emmeans 2022.

1299 **Figures and figure captions**

1300

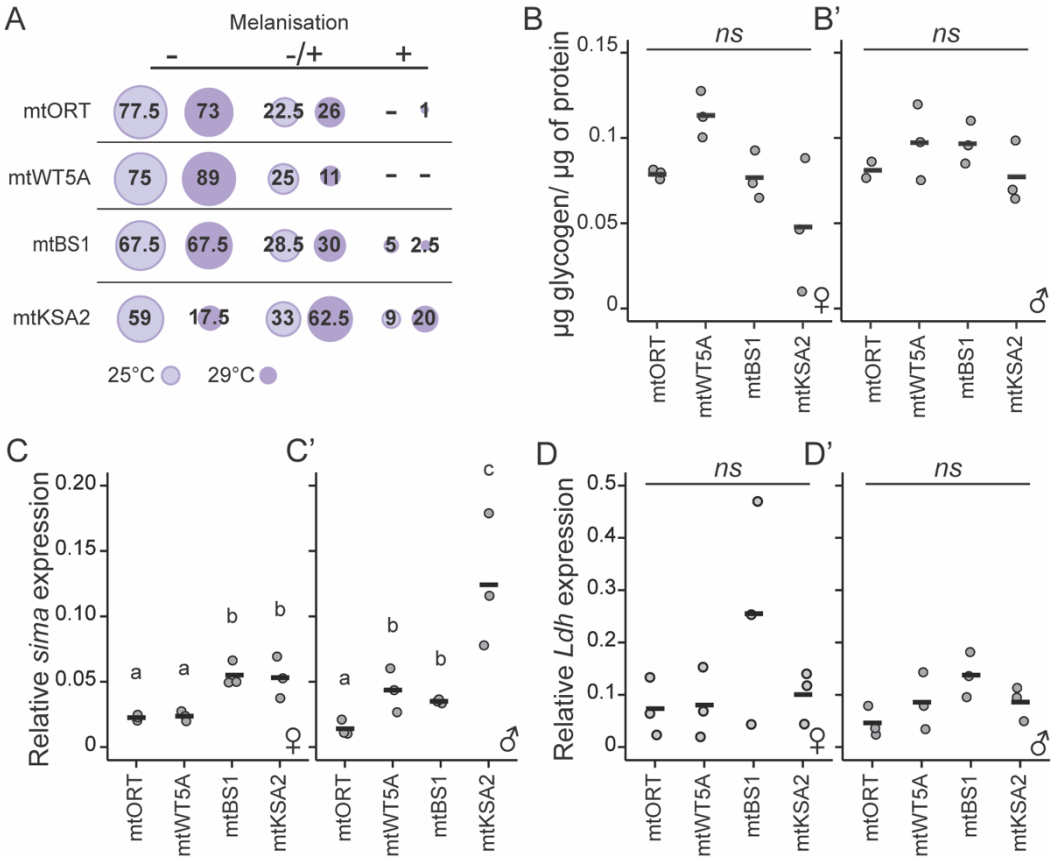

1301

1302 **Figure 1. mtDNA variation modulates the cell-mediated innate immune response in cybrid**
1303 **larvae. (A)** Cybrid larvae, reared at 25 °C or 29 °C, were exposed to *L. boulardi* parasitoid wasps
1304 and their ability to form a melanised capsule around the wasp larvae was measured (n=80). The
1305 success of the immune response was categorized as (-) a completely failed response with living,
1306 unmelanised wasp larva, (-/+) a partially successful response with partially melanised larva and (+) a
1307 successful response with completely melanised and encapsulated wasp larva (percentages). (**B-B'**)
1308 Glycogen levels of cybrid larvae were measured using a colorimetric analysis (n=3) and normalized
1309 to the amount of protein in the samples. (**C-D**) Expression of *sima* (**C-C'**) and *Ldh* (**D-D'**) in cybrid
1310 larvae (n=3) relative to the level of the control gene *His3.3b* expression (2^(-dCT)). The data in (**B-**
1311 **D**) were analysed with the Kruskal-Wallis test, pairwise comparisons were made using t-tests. Same
1312 letter indicates that there was no statistically significant difference, different letter indicates a
1313 statistical difference at the level of $p < 0.05$.

1314

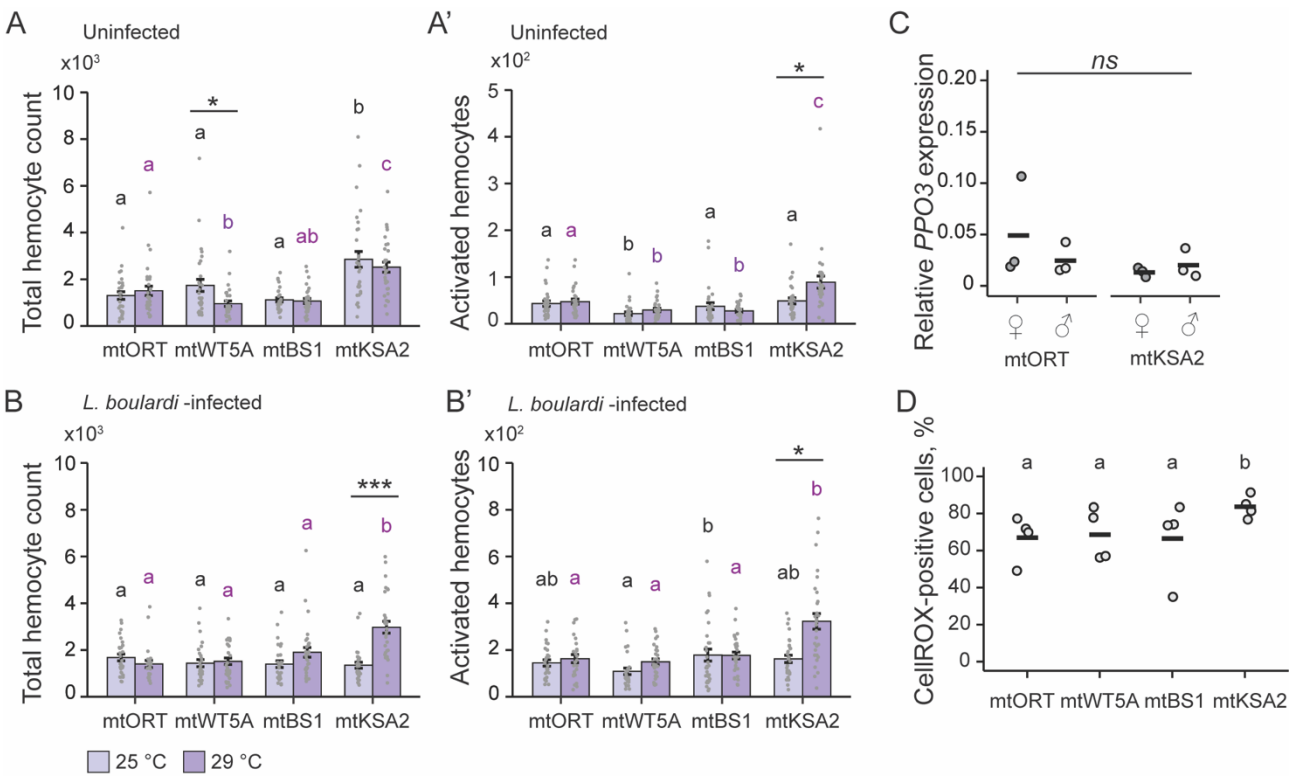

Figure 2. mtKSA2 larvae have elevated amount of hemocytes and ROS prior infection. (**A-B'**) Total amounts of hemocytes and hemocytes falling into the activated hemocyte gate were quantified in uninfected (**A-A'**) and wasp-infected (**B-B'**) cybrid larvae using a flow cytometer (n=30). Larvae were reared either at 25° C (light purple bars) or 29°C (dark purple bars). The data on hemocyte counts was analysed using a generalized linear model with negative binomial distribution, temperatures were analysed separately. Error bars indicate standard error of the mean. Black letters refer to the differences between the strains reared at 25 °C, purple letters at 29 °C. The underlined asterisks refer to differences between the two temperatures within a cybrid strain. (**C**) Expression of a lamellocyte specific gene, *PPO3*, was measured in the hemocytes of mtORT and mtKSA2 larvae reared at 29 °C, relative to the level of the expression of the control gene *His3.3b* expression (2^(-dCT)). (**D**) Reactive oxygen species (ROS) levels were measured in the hemocytes of non-infected 3rd instar cybrid larvae reared at 29 °C using the CellROX™ green reagent (n=4, around 2000 hemocytes were analysed per replicate) as a percentage of hemocytes stained with CellROX™. The data was analysed using logistic regression with a binomial distribution. Tukey post hoc tests were applied for pairwise comparisons between the strains. ns = not significant, * $p < 0.05$, ** $p < 0.01$, *** $p < 0.001$.

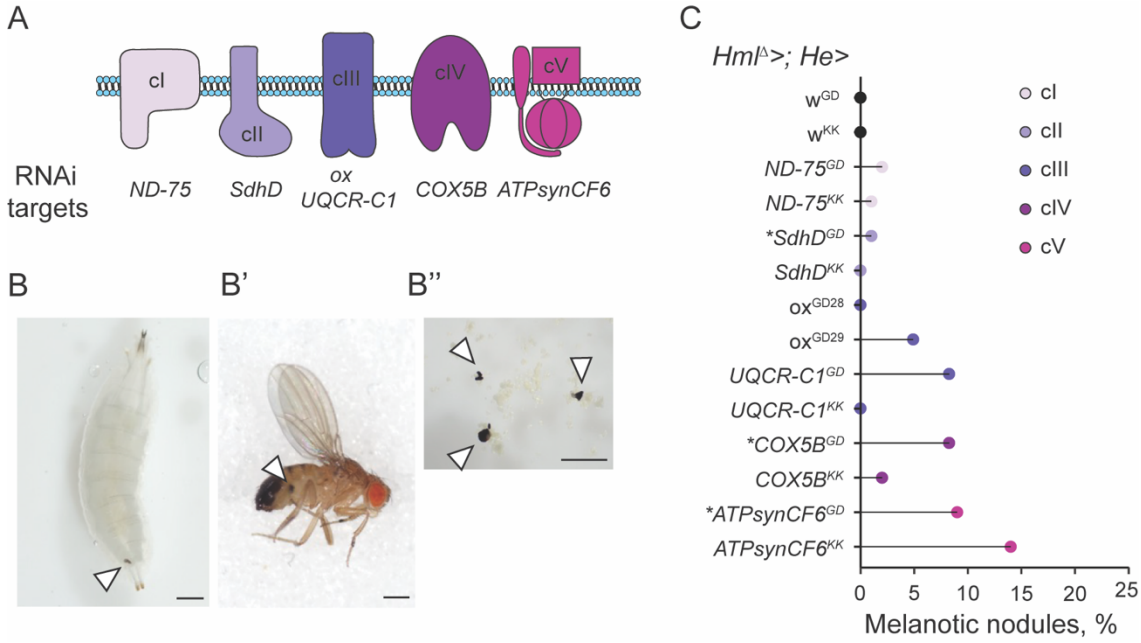

Figure 3. Knockdown of nuclear genes encoding for components of the mitochondrial OXPHOS complexes in hemocytes induces the formation of melanotic nodules. (**A**) A schematic presentation of oxidative phosphorylation (OXPHOS) complexes and the complex-specific nuclear encoded RNAi-induced knockdown target genes used in the experiments. (**B-B''**) Examples of melanotic nodules in *Hml$^{\Delta}$-GAL4;He-GAL4/UAS-ATPsynCF6^{GD}* in the (**B**) larval and (**B'**) adult stages, and (**B''**) melanotic nodules dissected from larva. Nodules are marked with an arrowhead. Scale bars 500 µm. (**C**) Quantification of melanotic nodules detected in the *Hml$^{\Delta}$-GAL4;He-GAL4/UAS-OXPHOS RNAi* larvae (n=100). The asterisks in front of the *ATPsynCF6^{GD}* and *SdhD^{GD}* constructs indicate that 1% of the driverless background control larvae (*w^{1118}/UAS-ATPsynCF6^{GD}*) also had melanotic nodules. (Schematic Figure **3A** modified from [4]).

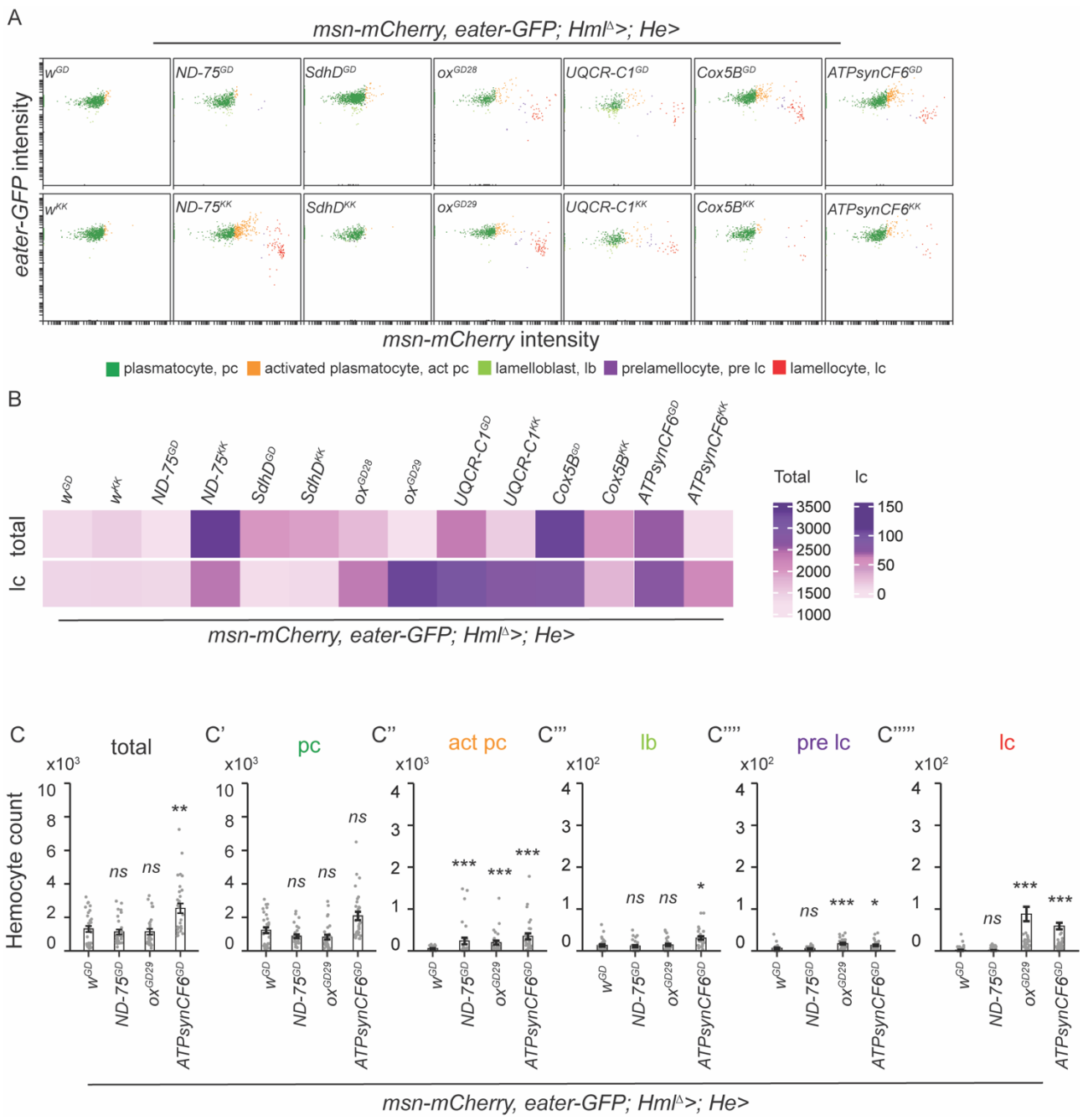

Figure 4. **Knockdown of nuclear encoded OXPHOS genes in hemocytes induces lamellocyte formation.** (**A**) Flow cytometry analysis of larval hemocytes using the plasmatocyte (*eater-GFP*, y -axis) and lamellocyte (*msn-mCherry,* x-axis) reporters showed that while the control animals (*msn-mCherry,eater-GFP;Hml$^{\Delta}$-GAL4;He-GAL4/w*) mainly had plasmatocytes, the knockdown of various OXPHOS genes induced the formation of lamellocytes (high mCherry intensity, marked in red). (**B**) A heatmap (n=30) showing the average total hemocyte and lamellocyte (lc) numbers in controls and in larvae with OXPHOS gene knockdown in hemocytes. (**C-C''''**) Quantification of total hemocytes and hemocyte types classified based on *eater-GFP* and *msn-mCherry* expression when knocking down the OXPHOS cI (*msn-mCherry,eater-GFP;Hml$^{\Delta}$-GAL4;He-GAL4/UAS-ND-75^{GD}*), cIII (*msn-*

1355 *mCherry,eater-GFP;Hml$^{\Delta}$-GAL4;He-GAL4/UAS-ox^{29GD}*) and cV (*msn-mCherry,eater-GFP;Hml$^{\Delta}$-*
1356 *GAL4;He-GAL4/UAS-ATPsynCF6^{GD}*) genes selected for further experiments (n=30). The data on
1357 hemocyte counts was analysed using a generalized linear model with a negative binomial distribution.
1358 Error bars indicate standard error of the mean. Asterisks indicate the statistical difference between
1359 the OXPHOS knockdowns and the control.
1360

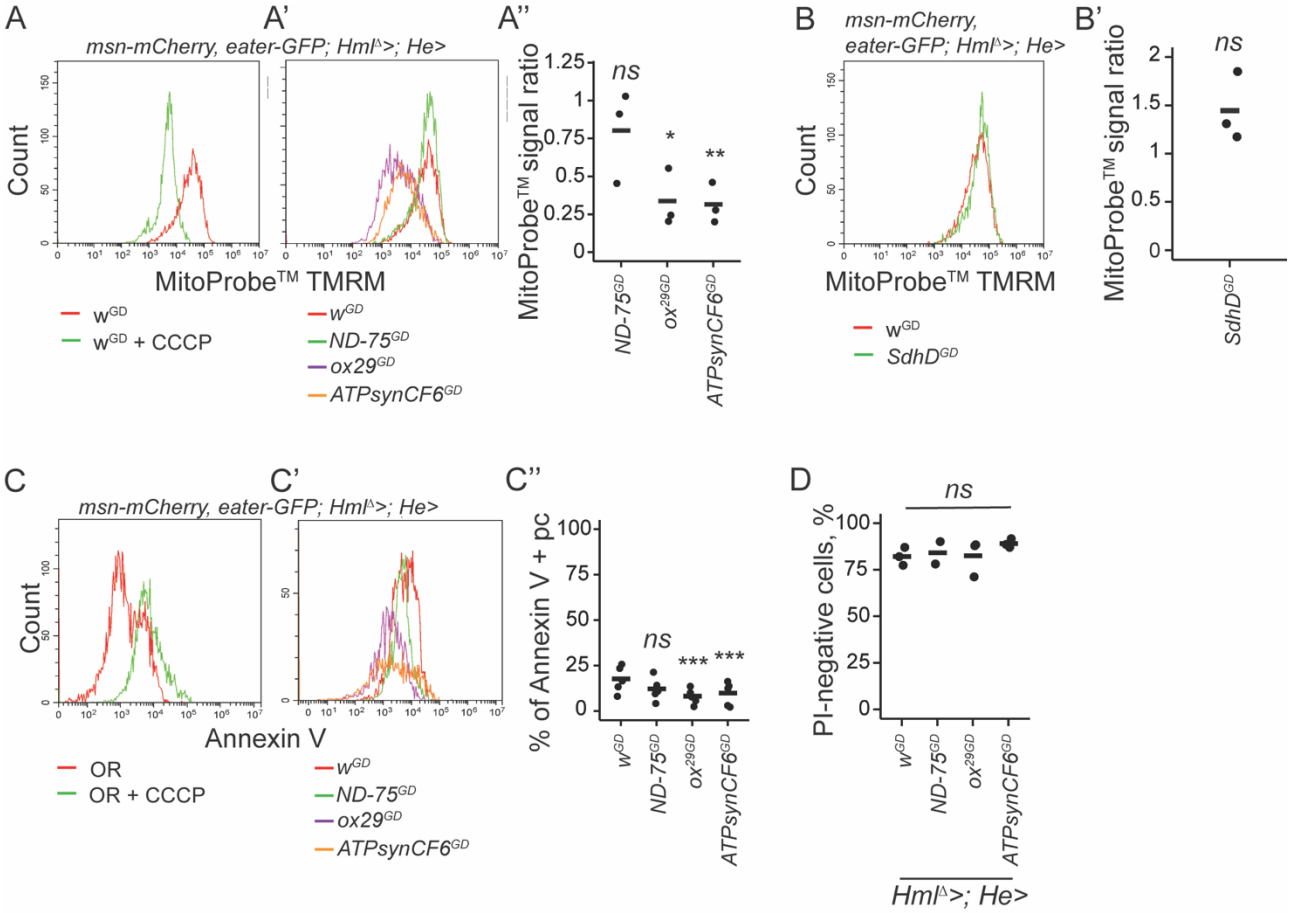

1361

1362 **Figure 5. Knocking down the selected cI, cIII and cV genes modulates the mitochondrial**
1363 **membrane potential and apoptosis in hemocytes. (A-A'''**) Mitochondrial membrane potential in
1364 hemocytes was measured using the MitoProbe^{TM} TMRM stain and a flow cytometer. (**A**)
1365 Mitoprobe^{TM} TMRM signal in control and Carbonyl cyanide *m*-chlorophenyl hydrazone (CCCP) -
1366 treated hemocytes. (**A'**) MitoProbe^{TM} TMRM signal in control plasmatocytes (*msn-mCherry,eater-*
1367 *GFP;Hml$^{\Delta}$-GAL4;He-GAL4/w^{GD}*) and in plasmatocytes with OXPHOS cI, cIII or cV gene
1368 knockdown (*msn-mCherry,eater-GFP;Hml$^{\Delta}$-GAL4;He-GAL4/UAS-OXPHOS RNAi*). (**A''**) The
1369 MitoProbe^{TM} TMRM signal was quantified as a ratio of the detected signal in the OXPHOS
1370 knockdown plasmatocytes to that of the control plasmatocytes, within a replicate experiment (n=3,
1371 2000-3500 *eater-GFP* positive plasmatocytes were analysed per replicate). (**B**) MitoProbe^{TM} TMRM

signal was also measured from the plasmatocytes of the *SdhD* hemocyte knockdown and control larvae, **(B')** and the signal was quantified as explained above (n=3, 2000-3500 plasmatocytes per replicate). The data was analysed using one-sample t-tests, comparing the ratios to a value of 1. (**C-C''**) Apoptosis was analysed by using an Annexin V -stain and a flow cytometer. (**C**) Annexin V Pacific Blue -conjugate signal in control and in CCCP -treated hemocytes. (**C'**) Annexin V Pacific Blue signal in control plasmatocytes (*msn-mCherry,eater-GFP;Hml$^{\Delta}$-GAL4;He-GAL4/w^{GD}*) and in plasmatocytes with OXPHOS gene silencing (*msn-mCherry,eater-GFP;Hml$^{\Delta}$-GAL4;He-GAL4/UAS-OXPHOS RNAi*). (**C''**) The data on apoptosis was quantified as a percentage of Annexin V pacific blue -positive plasmatocytes in a sample (n=4, 3000 plasmatocytes per replicate). The data was analysed using a logistic regression with a binomial distribution. (**D**) Proportion of live hemocytes (negative for PI staining) in controls and OXPHOS gene knockdown hemocytes (n=3, 5000-7000 hemocytes per replicate).

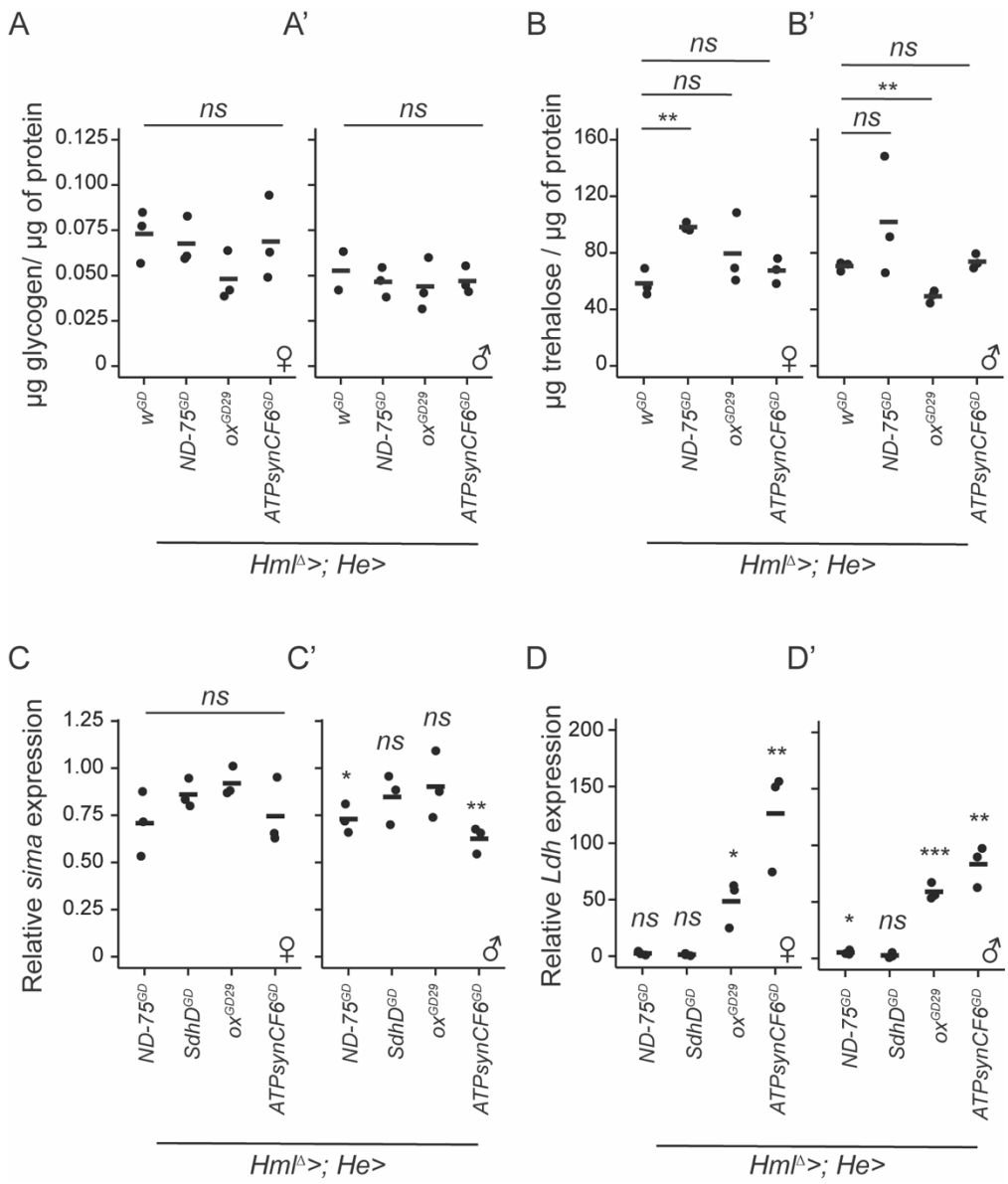

Figure 6. Knockdown of the OXPHOS genes in hemocytes does not cause major changes in glycogen nor trehalose levels, but cIII and cV knockdown induces *Ldh* expression. (A-A') Storage sugar glycogen content normalized to protein content in (**A**) female and (**A'**) male larvae with OXPHOS knockdown in hemocytes (n=3). (**B-B'**) Content of trehalose normalized to protein content in (**B**) female and (**B'**) male larval hemolymph (n=3). The data in (**A-B'**) were analysed using pairwise t-tests. (**C-D'**) Expression of (**C-C'**) *sima* and (**D-D'**) *Ldh* was measured in hemocytes of OXPHOS knockdown female and male larvae (n=3) and is shown here normalized to the expression of the control gene *His3.3b* expression, and relative to the expression level of *sima*/*Ldh* in the hemocytes of control animals. Data on overall differences were analysed using the Kruskal-Wallis test. When needed, pairwise differences were analysed using the t-test. ns = not significant, * $p < 0.05$, ** $p < 0.01$, *** $p < 0.001$.

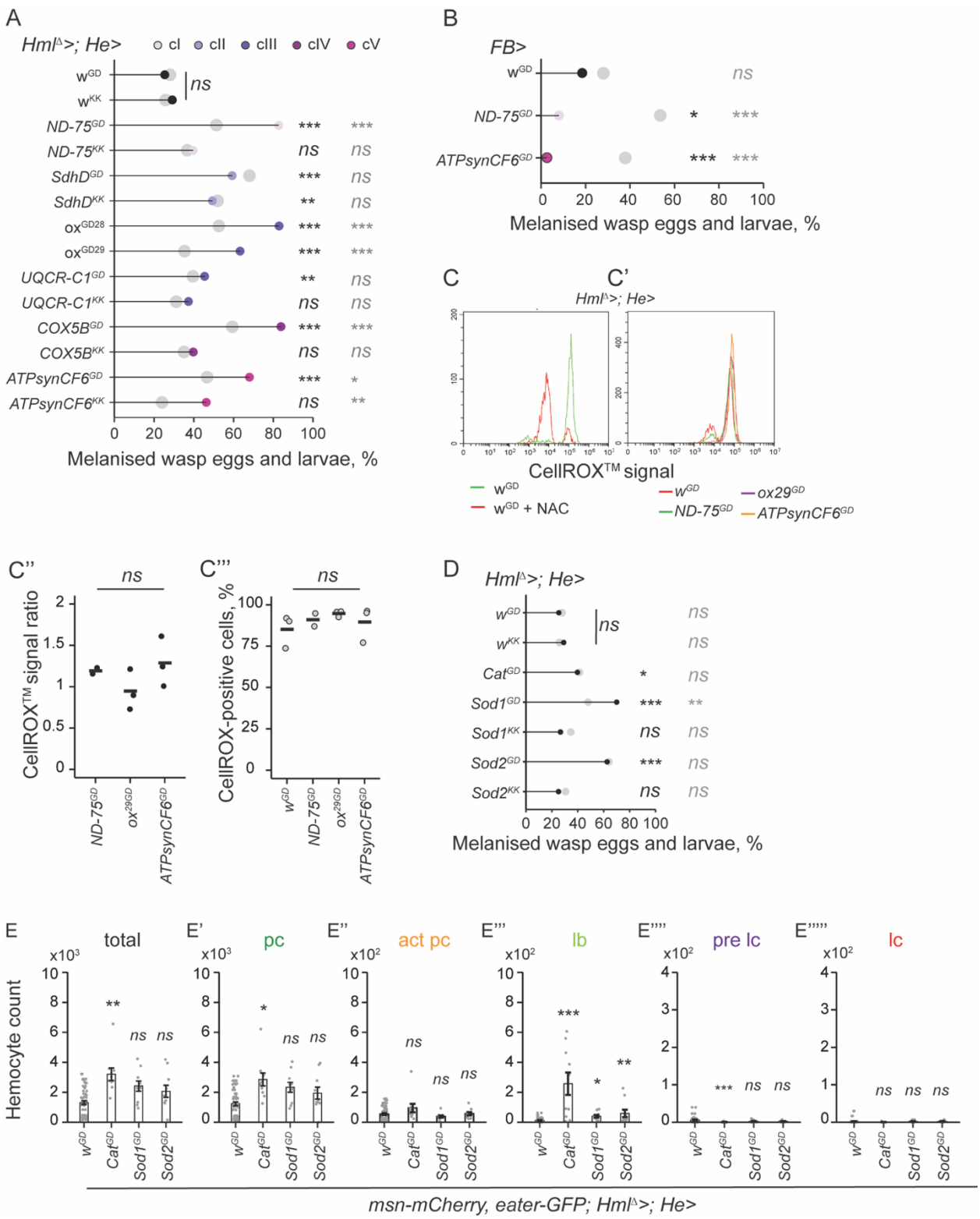

Figure 7. Knocking down genes of the OXPHOS complex I-V in hemocytes, but not in the fat body, results in an enhanced cell-mediated immune response. (**A**) Control larvae and larvae with OXPHOS gene knockdown in hemocytes were infected with *L. boulardi* wasps and the melanisation response against the wasp eggs and larvae was assessed (n=150). The plot shows the mean percentage of melanised larvae found in the control larvae (*Hml$^{\Delta}$-GAL4;He-GAL4/w*) in RNAi strain-specific

1409 controls (*w*^{1118}*/UAS-OXPHOS RNAi*) and in the larvae with OXPHOS knockdown in hemocytes
1410 (*Hml*$^{\Delta}$*-GAL4;He-GAL4/UAS-OXPHOS RNAi)*. (**B**) Melanisation response in the animals with *ND-75*
1411 and *ATPsynCF6* knockdown in the fat body (*FB-GAL4/UAS-OXPHOS RNAi*) (n=150). Colors in (**A**)
1412 and (**B**) refer to the OXPHOS complexes cI-cV. Grey circles indicate the percentage of melanised
1413 wasp eggs and larvae found in the RNAi strain -specific controls. Black asterisks indicate the
1414 difference in the OXPHOS knockdown compared to the general control (*Hml*$^{\Delta}$*-GAL4;He-GAL4/w)*
1415 and grey asterisks to the RNAi strain -specific controls. The data was analysed using logistic
1416 regression with a binomial distribution with replication as a random factor. (**C-C'''**) Reactive oxygen
1417 species (ROS) were measured using the CellROX™ Green reagent. (**C**) CellROX™ Green signal in
1418 controls and in hemocytes obtained from N-acetyl cysteine (NAC) -fed larvae. (**C'**) CellROX™
1419 Green signal in the control hemocytes (*Hml*$^{\Delta}$*-GAL4,He-GAL4/ w*^{GD}) and in the hemocytes with a
1420 knockdown of OXPHOS cI, cIII or cV genes. (**C''-C'''**) ROS levels were quantified as a ratio of the
1421 CellROX™ Green signal in the OXPHOS complex knockdown hemocytes to that of the control
1422 hemocytes (**C''**) and as a proportion of hemocytes positive for the CellROX™ Green signal (**C'''**)
1423 (n=3, 5000-7000 hemocytes per replicate). The ratios were analysed using one-sample t-tests,
1424 comparing the ratios to a value of 1. The percentages were analysed using a logistic regression with
1425 a binomial distribution. ns = not significant, * $p< 0.05$, ** $p< 0.01$, *** $p< 0.001$. (**D**) Control and
1426 antioxidant (AO) gene knockdown larvae were infected with *L. boulardi* wasps and the melanisation
1427 response against the wasp eggs and larvae was assessed (n=150). The plot shows the mean percentage
1428 (of three replications) of melanised wasp larvae found in the control larvae (*Hml*$^{\Delta}$*-GAL4;He-GAL4/w*
1429 and *w*^{1118}*/UAS-AO RNAi*) and in the larvae with antioxidant gene knockdown in hemocytes (*Hml*$^{\Delta}$*-*
1430 *GAL4;He-GAL4/UAS-AO RNAi)*. Grey circles indicate the percentage of melanised wasp larvae
1431 found in the RNAi strain -specific background controls (*w*^{1118}*/UAS-AO RNAi*). The data was analysed
1432 using logistic regression with a binomial distribution. Replication was included as a random factor in
1433 the analyses. Black asterisks indicate the difference between *Hml*$^{\Delta}$*-GAL4;He-GAL4/AO RNAi* and
1434 the *Hml*$^{\Delta}$*-GAL4;He-GAL4/w* controls and grey asterisks indicate the difference between the
1435 knockdown sample and the specific background control. (**E-E'''''**) Quantification of total hemocytes
1436 and hemocyte types classified based on *eater-GFP* and *msn-Cherry* expression when knocking down
1437 the AO genes in hemocytes (n=10). Of note, control samples are the same as in Figure 4 C-C'''''
1438 (n=30). Asterisks indicate the statistical difference between the AO knockdowns and the control.
1439 Error bars indicate standard error of the mean. The data on hemocyte counts was analysed using a
1440 generalized linear model with a negative binomial distribution. ns = not significant, * $p< 0.05$, ** $p<$
1441 0.01, *** $p< 0.001$.

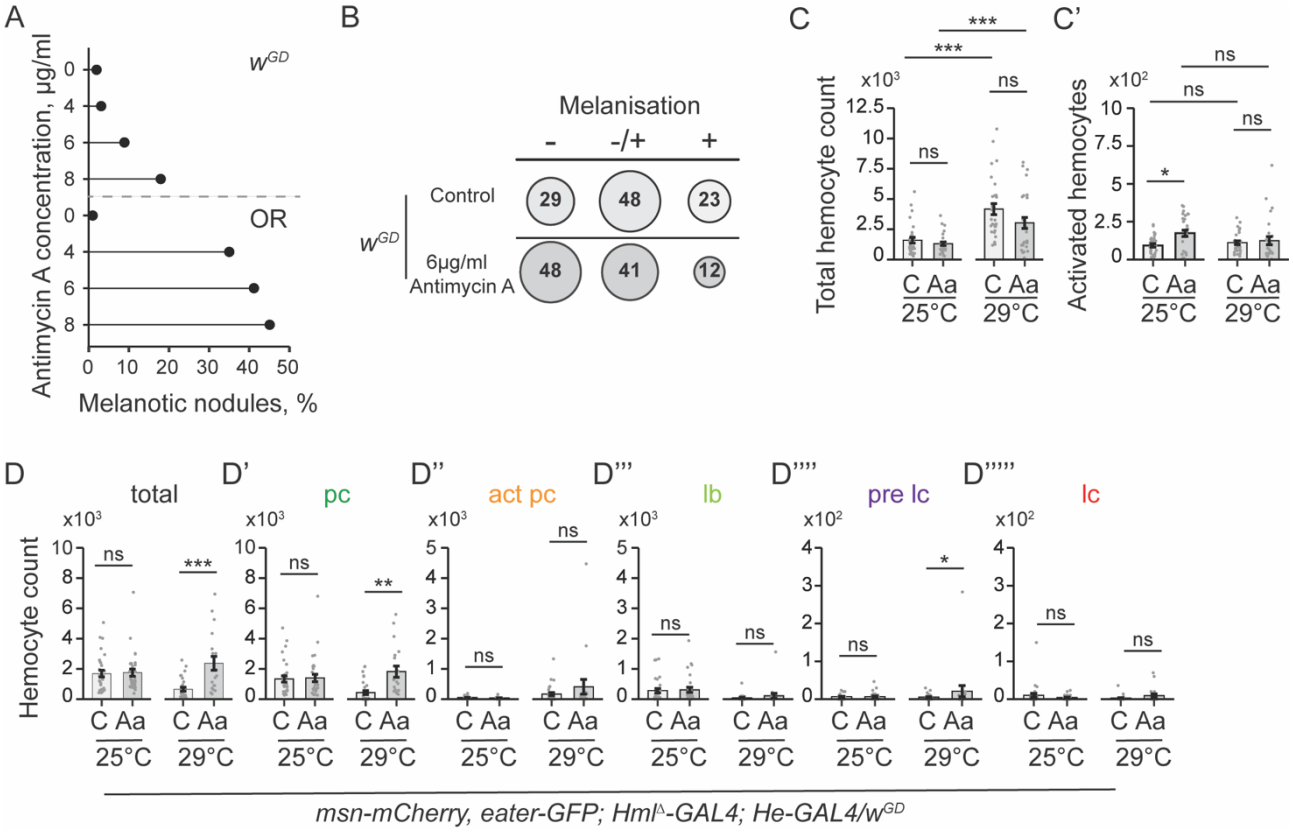

Figure 8. **Pharmacological inhibition of OXPHOS complex III partially phenocopies the effects of the mtKSA2 mutation and the OXPHOS gene knockdown in hemocytes.** (**A**) Genetic background strains of the cybrids (ORT) and the OXPHOS RNAi lines (w^{GD}) were fed with different concentrations of antimycin A (Aa) in their food medium and its effect on the formation of melanotic nodules was examined (n=100/treatment) in 3rd instar larvae. Since ORT larvae were sensitive to the antimycin A (high melanotic nodule incidence even at low concentration), we selected w^{GD} for the follow-up experiments. (**B**) The response of antimycin A fed (6 µg/ml in the food medium, n=86) and control w^{GD} larvae (n=100) against *L. boulardi* parasitoid wasps assessed as a proportion of melanised parasitoids at 29 °C (n=. **(C-C')** Total amounts of hemocytes and hemocytes falling into the activated hemocyte gate were measured in uninfected 3rd instar w^{GD} larvae using a flow cytometer (n=30). C = control larvae reared on normal fly food medium; Aa = larvae reared on 6 ug/ml antimycin A in the food. (**D-D'''''**) Quantification of total hemocytes and hemocyte types classified based on *eater-GFP* and *msn-mCherry* expression when rearing the larvae on 6 µg/ml antimycin A in their food medium (n = 30). Error bars indicate standard error of the mean. The data on hemocyte counts was analysed using a generalized linear model with a negative binomial distribution. Asterisks indicate the statistical difference of the result: ns = not significant, * p< 0.05, ** p< 0.01, *** p< 0.001.

1460

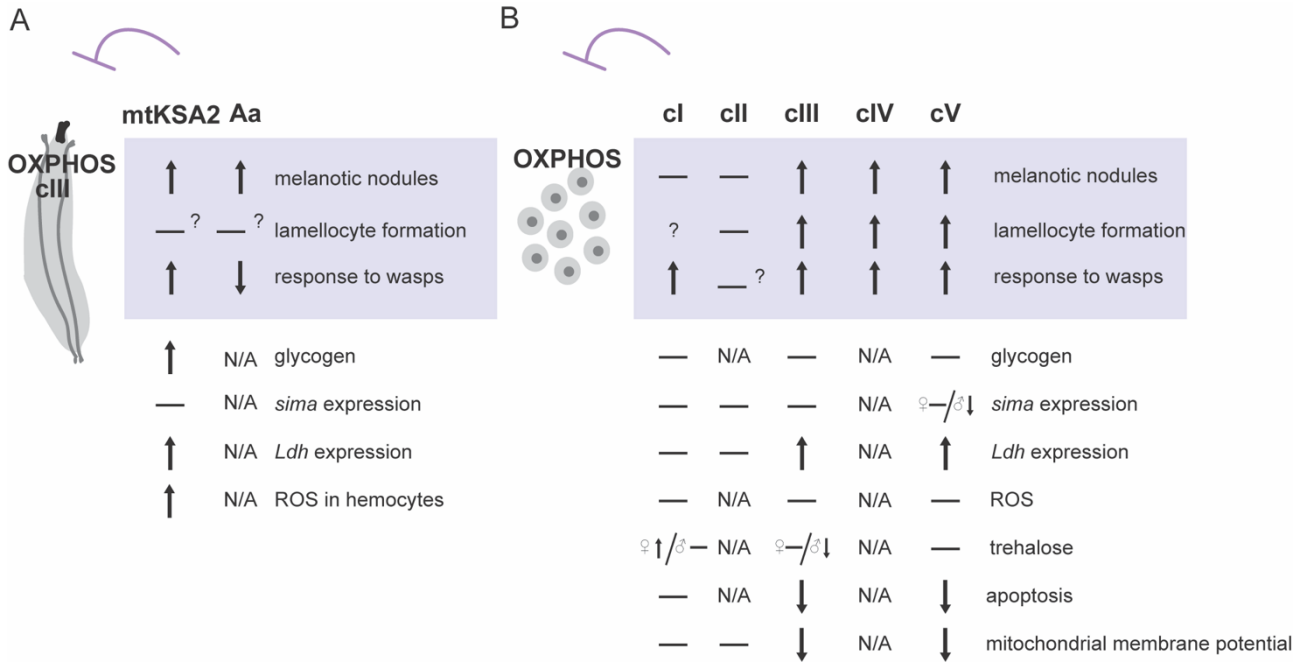

1461

1462 **Figure 9. Summarized main findings.** Illustration summarizing the effects of OXPHOS
1463 perturbation (**A**) ubiquitously and (**B**) hemocyte-specifically. (**A**) Ubiquitous alterations were
1464 achieved by introgressing mtDNA variant mtKSA2 with a mutation in the OXPHOS cIII gene
1465 *cytochrome b* and three control mtDNA variants into the Oregon-RT (ORT) background, as well as
1466 by feeding the ORT and w^{1118} larvae with the cIII inhibitor antimycin A. (**B**) Hemocyte-specific
1467 OXPHOS modulation was achieved by knocking down the nuclear encoded genes *ND-75*, *SdhD*, *ox*
1468 *COX5B* and *ATPsynCF6* coding for OXPHOS cI-cV subunits, respectively, using a hemocyte specific
1469 GAL4 (*He-GAL4;Hml$^{\Delta}$-GAL4*) and the RNA interference method. The main experiments were
1470 conducted by knocking down the target genes from cI, cIII and cV using RNAi strains from the
1471 VDRC GD-library, and the immune-related phenotypic findings are outlined in the box. In the case
1472 of antimycin A, only immune-related phenotypes were assessed. Of note, mtKSA2 melanotic nodule
1473 phenotype was shown in [23]. The direction of the changes is indicated with arrows, horizontal lines
1474 indicate no change, N/A indicates that the line was not included in the experiment. In cases where
1475 males and females were tested separately the direction of the possible sex specific change is marked
1476 separately for both sexes.

1477